Article

Tropical response to ocean circulation slowdown raises future drought risk

https://doi.org/10.1038/s41586-025-09319-x

Received: 11 May 2023

Accepted: 20 June 2025

Published online: 30 July 2025

Check for updates

Pedro N. DiNezio[1]✉, Timothy M. Shanahan[2], Tianyi Sun[3], Chijun Sun[4], Xian Wu[5], Allison Lawman[6], David Lea[7], Masa Kageyama[8], Ute Merkel[9], Matthias Prange[9], Bette Otto-Bliesner[10] & Xu Zhang[11]

Projections of tropical rainfall under global warming remain highly uncertain[1,2], largely because of an unclear climate response to a potential weakening of the Atlantic meridional overturning circulation (AMOC)[3]. Although an AMOC slowdown can substantially alter tropical rainfall patterns[4–8], the physical mechanisms linking high-latitude changes to tropical hydroclimate are poorly understood[11]. Here we demonstrate that an AMOC slowdown drives widespread shifts in tropical rainfall through the propagation of high-latitude cooling into the tropical North Atlantic. We identify and validate this mechanism using climate model simulations and palaeoclimate records from Heinrich Stadial 1 (HS1)—a past period marked by pronounced AMOC weakening[9,10]. In models, prevailing easterly and westerly winds communicate the climate signal to the Pacific Ocean and Indian Ocean through the transport of cold air generated over the tropical and subtropical North Atlantic. Air–sea interactions transmit the response across the Pacific Ocean and Indian Ocean, altering rainfall patterns as far as Indonesia, the tropical Andes and northern Australia. A similar teleconnection emerges under global warming scenarios, producing a consistent multi-model pattern of tropical hydroclimatic change. These palaeo-validated projections show widespread drying across Mesoamerica, the Amazon and West Africa, highlighting an elevated risk of severe drought for vulnerable human and ecological systems.

Several mechanisms have been proposed to explain tropical climate changes driven by localized cooling over the North Atlantic due to a reduction in the Atlantic meridional overturning circulation (AMOC) strength[11]. Among them, a well-established theory predicts that the hemispheric energy imbalance caused by a change in the strength of the AMOC would produce a north–south shift in the Inter-Tropical Convergence Zone (ITCZ)[7]—the belt of strong rainfall and converging winds encircling the tropics. Global climate models produce a shift in the ITCZ towards the Southern Hemisphere in response to a weaker AMOC and the associated North Atlantic cooling. However, outside the circum-tropical Atlantic, the simulated changes seem to be model-dependent and show notable departures from a zonally symmetric response[5,6,8,12]. These model differences suggest more complex pathways and mechanisms linking the global tropics to variations in AMOC strength and the associated inter-hemispheric distribution of heat[11].

The climatic impacts and mechanisms of a weaker AMOC cannot be studied using historical records because current observations show trends that are too small to be discernible[13–15]. Furthermore, the detection of hydrological responses using instrumental observations would probably be obscured by responses to other hemispheric forcings, such as changing aerosol emissions. Past climate intervals, such as Heinrich stadials, provide an alternative target for model validation, because it is well established that the AMOC was weaker during these cooling events in the North Atlantic[9,10,16]. Moreover, palaeoclimate records from past Heinrich stadials show pronounced changes in hydroclimate across the global tropics, but, as in the models, the patterns of rainfall change inferred from these palaeodata cannot be explained by a simple southward shift of the ITCZ[17]. Alternative mechanisms have been considered[5,6,8,11], but a rigorous and systematic evaluation against palaeoclimatic evidence has not been performed on a global scale.

To address these issues, we studied the tropical response to reductions in AMOC strength using ensembles of climate model simulations combined with a synthesis of hydroclimate changes during Heinrich Stadial 1 (HS1)—the best sampled geological interval, about 15–17 ka BP, with robust and unambiguous evidence of a weaker AMOC[9,10]. The term 'Heinrich stadial' has been introduced to identify the interval associated with a Heinrich event in regions, such as the tropics, where climatic signals exceed the duration of the ice-rafted debris events[18]. To identify mechanisms explaining changes during HS1, we used a multi-model ensemble of simulations of the climate response to a weaker AMOC.

[1]Department of Atmospheric and Oceanic Sciences, University of Colorado Boulder, Boulder, CO, USA. [2]Department of Earth and Planetary Sciences, Jackson School of Geosciences, The University of Texas at Austin, Austin, TX, USA. [3]Environmental Defense Fund, Austin, TX, USA. [4]Earth and Planetary Sciences Department, University of California, Davis, Davis, CA, USA. [5]The Department of Sustainable Earth Systems Sciences, The University of Texas at Dallas, Richardson, TX, USA. [6]Environmental Studies and Science Program, Colorado College, Colorado, Springs CO, USA. [7]Department of Earth Science, University of California, Santa Barbara, CA, USA. [8]Laboratoire des Sciences du Climat, l'Environnement/Institut Pierre-Simon-Laplace, Gif-sur-Yvette, France. [9]MARUM—Center for Marine Environmental Sciences, University of Bremen, Bremen, Germany. [10]Climate and Global Dynamics Division, National Center for Atmospheric Research, Boulder, CO, USA. [11]British Antarctic Survey, Cambridge, UK. ✉e-mail: pedro.dinezio@colorado.edu

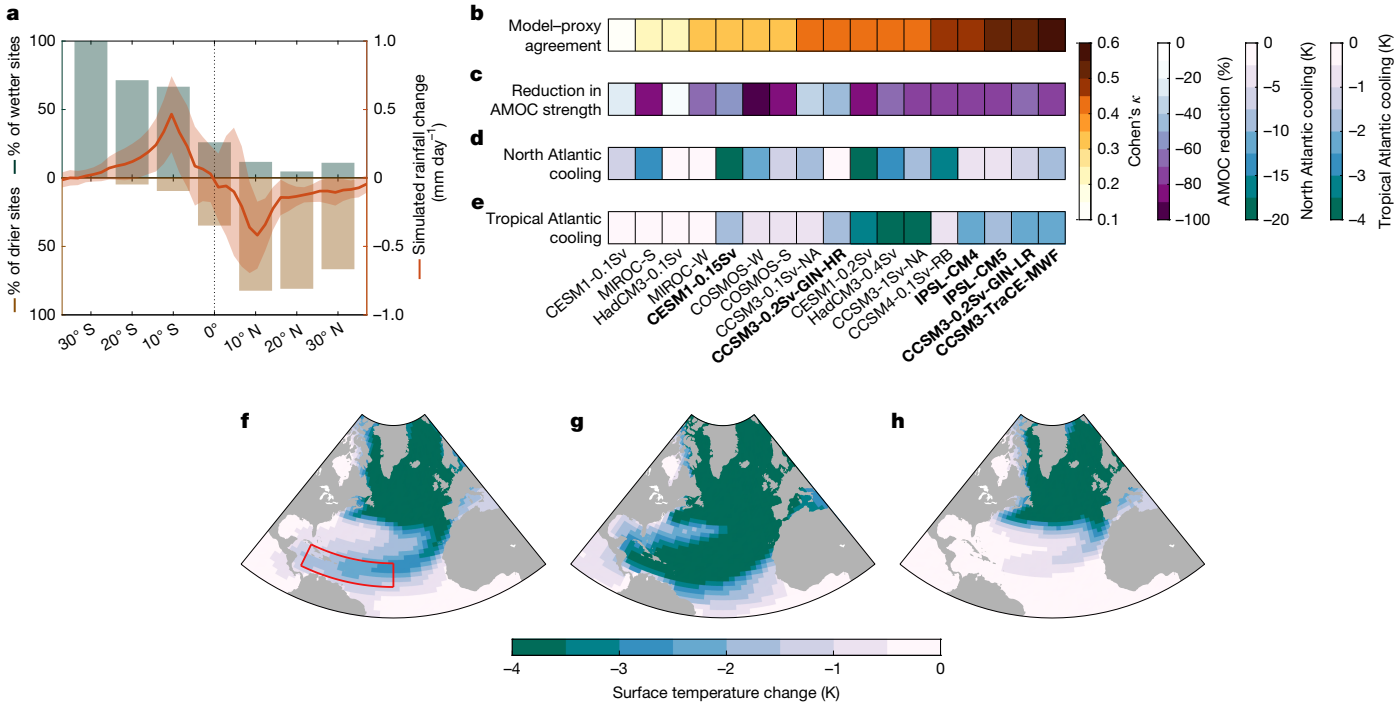

Fig. 1 | Proxy-inferred changes in hydroclimate during HS1 compared with simulated changes in response to reductions in the strength of the AMOC. **a**, Latitudinal patterns of rainfall change simulated in response to reductions in AMOC strength (red line and shading) and during HS1 inferred from rainfall-sensitive proxies (bars). Shading indicates the range of maximum and minimum of the simulated rainfall changes among all models. Proxy-inferred changes (bars) are estimated as the percentage of sites with a wetter or drier HS1 within each 10° latitude band. **b**, Agreement between simulated and proxy-inferred patterns of rainfall change based on the Cohen's κ metric[19]. The simulations, listed along the horizontal axis, are sorted by level of agreement from low (left) to high (right). **c**, Simulated reduction in AMOC as a percentage of the strength in the glacial control. **d**, Simulated surface air temperature change averaged over the high-latitude North Atlantic (60° W–0° 40° N–65° N). **e**, Simulated surface air temperature change averaged over the tropical North Atlantic (80° W–40° W 12° N–22° N). **f**–**h**, Simulated surface air temperature changes grouped by the magnitude of the cooling response over the tropical North Atlantic (domain outlined in red in **f**): between −3 K and −1 K (moderate), exceeding −3 K (strong) and less than −1 K (muted). Simulations with moderate cooling are identified with bold labels in **e**. See Extended Data Table 1 for a list of the simulations, including their categorization according to the patterns of cooling.

These simulations were run under Last Glacial Maximum (LGM) boundary conditions to best approximate the mean state of the climate system before the onset of HS1 (Methods). AMOC reductions were simulated by applying a flux of freshwater over different regions in the North Atlantic. The resulting ensemble of hosing simulations exhibits a broad range of reductions in AMOC strength and cooling responses over the high-latitude North Atlantic (Extended Data Fig. 1). Although differences in the experimental design do not allow us to systematically explore the impacts of glacial boundary conditions and the rates and locations of freshwater forcing, the ensemble provides diverse patterns of rainfall change for model evaluation against the palaeodata (Extended Data Fig. 2). Further details on the ensemble are provided in Supplementary Information section 1.

We focused our analysis on HS1 because the background state for this event is relatively better known and closer to full glacial conditions as in our simulations, than the Younger Dryas, allowing for a more direct comparison against our ensemble and because records spanning earlier Heinrich stadials are too sparse to accurately capture the spatial patterns of past rainfall change. The simulated responses with the highest agreement with the palaeodata were used to identify mechanisms linking changes in the North Atlantic with the global tropics. These mechanisms were then identified in multi-model projections to constrain future changes in tropical rainfall associated with reductions in AMOC strength.

Past patterns of hydroclimate change

Our methodology for reconstructing hydroclimate changes during HS1 includes several new features that are important for quantitative proxy–model evaluation. The abundance of rainfall-sensitive records (>200) spanning the HS1 interval allowed us to apply very stringent selection criteria to reconstruct patterns of change during HS1 and assess the robustness of our conclusions to proxy interpretation (Methods). Record selection focused on temporal resolution and length to resolve changes during HS1 relative to a glacial or deglacial baseline. Sufficient temporal resolution (at least 5 data points during the HS1 interval) was important to exclude records in which climate or proxy noise might be aliased into a millennial-scale signal. Record length extending the LGM (21–19 ka) was important to make sure that each selected record can capture the HS1 response directly linked to a weaker AMOC relative to other deglacial drivers. This is an important consideration for comparison against the simulations, which by construction isolate the response to AMOC reductions. Previous work[17] inferred changes relative to a Holocene baseline, conflating responses to different deglacial forcings. The application of our selection criteria resulted in a total of 125 records of rainfall-sensitive proxies and 113 merged sites spanning the global tropics (Extended Data Fig. 3).

The patterns of hydroclimate change inferred from our synthesis are largely independent of the proxy techniques used to infer past changes. All records are based on proxies with well-established relationships to rainfall, including 54 records based on terrestrial water isotopes and 51 records based on aridity proxies—that is, dust flux, terrigenous discharge or high-resolution lake-level reconstructions. Sensitivity analysis shows that these records alone can reconstruct the bulk of the spatial patterns needed to validate and detect model responses (Extended Data Fig. 4). The remaining 20 records are based on vegetation proxies (carbon isotope ratios and pollen), also reflective of

hydroclimate changes. We excluded marine isotopic records measuring $\delta^{18}O$ of seawater from foraminifera from our analysis because of their more complex relationship to precipitation, evaporation and oceanic advection. Moreover, owing to the difficulties in extracting quantitative data from most of these proxy reconstructions, the changes at each site were categorized as drier, unchanged or wetter during HS1 relative to the glacial or deglacial baseline following previous work[19]. The categorization was done largely following the original published interpretation of the records. A limited subset of 23 records required new interpretation largely because the original authors did not identify changes during HS1. We changed the interpretation of a small subset of 6 records because of an ambiguous HS1 change. Further details are provided in Supplementary Information section 2. Our reinterpretation of these records improved the delineation of patterns by identifying many sites with an unchanged HS1 hydroclimate. The resulting network of sites with hydroclimate changes was used to validate model responses, quantifying agreement with simulated patterns using Cohen's κ metric[19] (Methods).

Our proxy data synthesis for HS1 shows broadly coherent patterns across the global tropics, with most sites showing drier conditions in the Northern Hemisphere and wetter conditions in the Southern Hemisphere, consistent with a southward-shifted ITCZ (Fig. 1a). However, regional differences in the simulated hydroclimatic responses are also evident, particularly away from the tropical Atlantic (Extended Data Fig. 2), suggesting that other mechanisms are important for transmitting the signal from the Atlantic to the global tropics. Differences in the ability of models to simulate these regional responses are evident in the large variations in the proxy–model agreement (Fig. 1b), with some models showing poor agreement ($\kappa = 0.07$ for CESM1-0.1Sv) and others simulating highly consistent proxy–model responses ($\kappa = 0.57$ for CCSM3-TraCE-MWF). Although these differences could arise from the intensity of the responses to freshwater forcing, we do not find a consistent relationship between the level of proxy–model agreement on the magnitudes of the AMOC reduction or the magnitude of high-latitude cooling (Fig. 1c,d). Instead, we see the highest proxy–model agreement for simulations with cooling in the tropical North Atlantic and conversely the lowest agreement for those exhibiting muted cooling in this region (Fig. 1e). There are a few exceptions to this relationship (for example, CCSM4-0.1Sv-RB and CESM1-0.15Sv) suggesting that models simulate distinct hydrological responses depending on the magnitude of cooling over the tropical North Atlantic. The robustness of this link is supported by a significant correlation ($r = 0.53$, $P < 0.03$, $N = 17$) between the values of global proxy–model agreement (measured by κ) and the magnitude of tropical cooling over the North Atlantic across all 17 simulations in our ensemble (Extended Data Fig. 5a). Higher correlations are obtained when we exclude the three simulations with the strongest cooling ($r = 0.71$, $P < 0.03$, $N = 14$). By contrast, cooling in the high-latitude North Atlantic does not explain the levels of proxy–model agreement in our full ensemble (Extended Data Fig. 5b, $r = 0.07$, $P < 0.79$, $N = 17$).

Evaluation of simulated responses

Our simulations indicate that the extent of cooling over the tropical North Atlantic is driven by distinct patterns of AMOC-induced cooling. We used ensemble averaging to isolate common responses to the distinct patterns of cooling (Extended Data Table 1). Simulations with a moderate temperature response show the cooling pattern in the North Atlantic extending southwestward from the Iberian Peninsula into the westernmost tropical North Atlantic and the Caribbean Sea, where cooling ranges from −1 K to −3 K (Fig. 1f, domain outlined in red). The rainfall changes in these moderate cooling simulations capture many features seen in the palaeodata (Fig. 2a), leading to the highest model-data agreement, to our knowledge, across the global tropics, with $\kappa = 0.58$ based on the ensemble mean pattern of the moderate

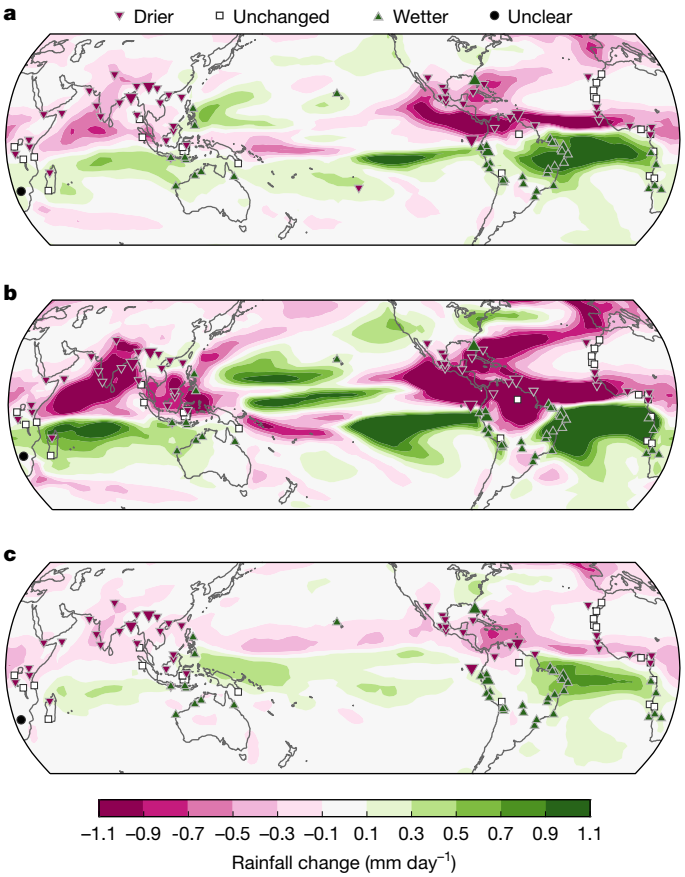

Fig. 2 | Rainfall responses associated with patterns of tropical Atlantic cooling. a–c, Ensemble mean changes in the annual mean rainfall averaged across simulations with moderate (**a**), strong (**b**) and muted (**c**) cooling. Symbols indicate changes inferred from palaeoclimate records. Bigger triangles indicate sites resulting from merging multiple records within a 100-km radius. The simulations used to compute each response are listed in Extended Data Table 1.

cooling simulations. The superior agreement in this ensemble suggests that the associated pattern of cooling in the tropical North Atlantic is important for explaining hydroclimate changes during HS1. A similar pattern of cooling is present in another subset of simulations, but we distinguish them here because the magnitude of cooling over the Caribbean and tropical Atlantic is unrealistically large (Fig. 1g) compared with palaeodata (Extended Data Fig. 6 and Supplementary Information section 3). These strong cooling simulations exhibit lower levels of agreement with $\kappa = 0.47$ for the ensemble mean rainfall response. The excessive temperature response (larger than 3 K in the outlined domain in Fig. 1f) produces drying with broader spatial extent than is evident in the proxy data in regions such as the Amazon and the Maritime Continent (Fig. 2b). A third set of simulations show the high-latitude cooling response characteristic of an AMOC collapse, but the pattern does not propagate over to the tropical North Atlantic and Caribbean (Fig. 1h, average cooling less than 1 K over the outlined domain). These muted cooling simulations produce weaker tropical rainfall responses with patterns that are inconsistent with the palaeoclimate data (Fig. 2c). For instance, they do not simulate wetter conditions over northern Australia nor along the spine of the tropical Andes as seen in proxies, resulting in lower agreement ($\kappa = 0.37$).

Most simulations show a substantial degree of agreement with the palaeoclimate data globally because they simulate a southward ITCZ shift in the Atlantic, with a pattern of drying north of the equator and wetter conditions to the south that is also evident in the palaeodata

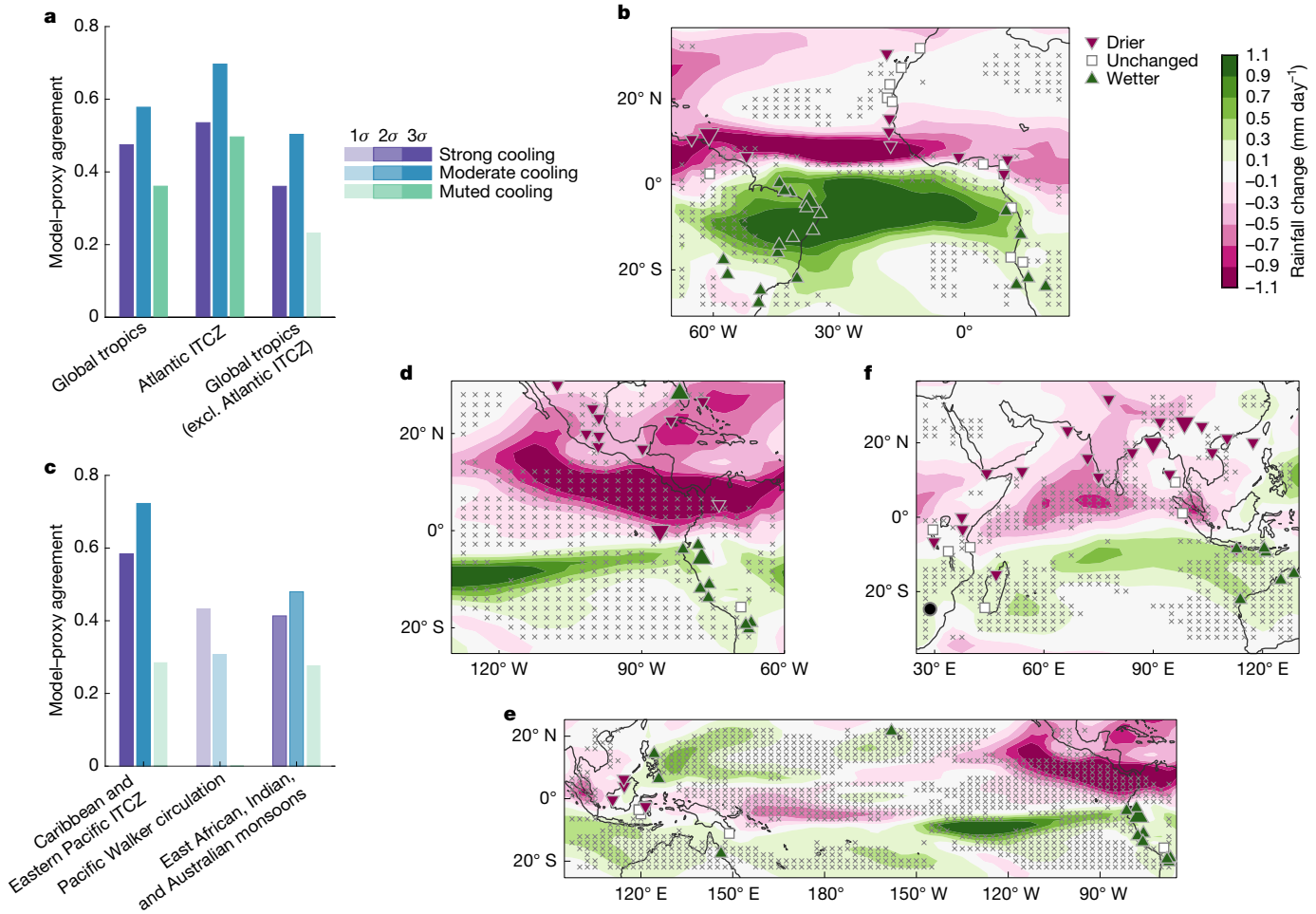

Fig. 3 | Simulated climate responses driving hydroclimate changes during HS1. a,**c**, Pattern agreement between simulated and proxy-inferred changes in rainfall in several domains as a function of the magnitude of cooling over the tropical North Atlantic. Shading indicates different levels of statistical significance of the κ metric. The regions used for agreement are outlined in the Methods. **b**,**d**–**f**, Simulated and proxy-inferred rainfall changes associated with a series of climatic responses driven by moderate cooling over the tropical Atlantic and Caribbean Sea: Atlantic ITCZ (**b**), Caribbean and Eastern Pacific ITCZ (**d**), Pacific Walker Circulation (**e**) and East African, Indian, and Australian Monsoons (**f**). The simulated changes (shading) are the average among the six simulations exhibiting moderate cooling over the tropical Atlantic and Caribbean Sea (80° W–40° W 12° N–22° N). The proxy-inferred changes (symbols) are given in categorical form—that is, drier, wetter or unchanged HS1 relative to the deglacial baseline. Hatching indicates regions in which the multi-model response under moderate North Atlantic cooling has a different sign than the response for muted North Atlantic cooling.

(Fig. 2). Similar levels of agreement are found when the model-data agreement is quantified over the circum-tropical Atlantic (Fig. 3a). This result is consistent with theory and indicates that the southward shift of the Atlantic ITCZ is controlled by the large temperature responses in the high-latitude North Atlantic, with a lesser role for temperature responses in the tropics. When we exclude the tropical Atlantic from the global domain, the κ values are higher and more statistically significant ($P < 0.01$) for simulations with moderate cooling in the tropical North Atlantic than for those with muted or strong cooling (Fig. 3a). This confirms the importance of this temperature response in communicating the influence of an AMOC collapse to the global tropics. Higher regional κ values are found in the Pacific Ocean and Indian Ocean for the ensemble of models with moderate cooling (Fig. 3c). This response shows higher agreement because it produces widespread drying in the eastern Pacific margin of Central and South America, extending southward along the Andes and western South America. In the Central Andes, the hydroclimate response reverses sign, consistent with the evidence for wetter conditions and higher lake levels during HS1 (Fig. 3c,d, triangles). Across the Pacific, proxies from Borneo and Sulawesi suggest decreased precipitation over the Maritime Continent (Fig. 3e, triangles), although less spatially coherent proxy and model changes lead to levels of agreement with lower, 1σ, statistical significance than the other regions (Fig. 3c). In the Indian Ocean region, models with moderate (and strong) cooling over the tropical Atlantic produce drying north of the equator and wetter conditions to the south, including over northern Australia (Fig. 3f, shading) in agreement with the proxy evidence (Fig. 3f, triangles). By contrast, the models with muted tropical cooling do not produce increased rainfall over northern Australia and have more limited drying over India (Fig. 3f, stippling), explaining the lower and less significant κ values.

Mechanisms driving tropical response

Our simulations show that the Pacific response is initiated when the cooling pattern in the tropical Atlantic reaches the Caribbean Sea and extends across the Central American Isthmus into the Pacific Ocean. The cooling pattern is communicated across land through the transport of cold air by the prevailing trade winds as proposed by previous works[20,21]. Cooling north of the equator induces a response to the south of it in the eastern tropical Pacific characterized by ocean warming and increased rainfall extending to 20° S along coastal South America and the tropical Andes (Fig. 4a,b). The southward extent and magnitude

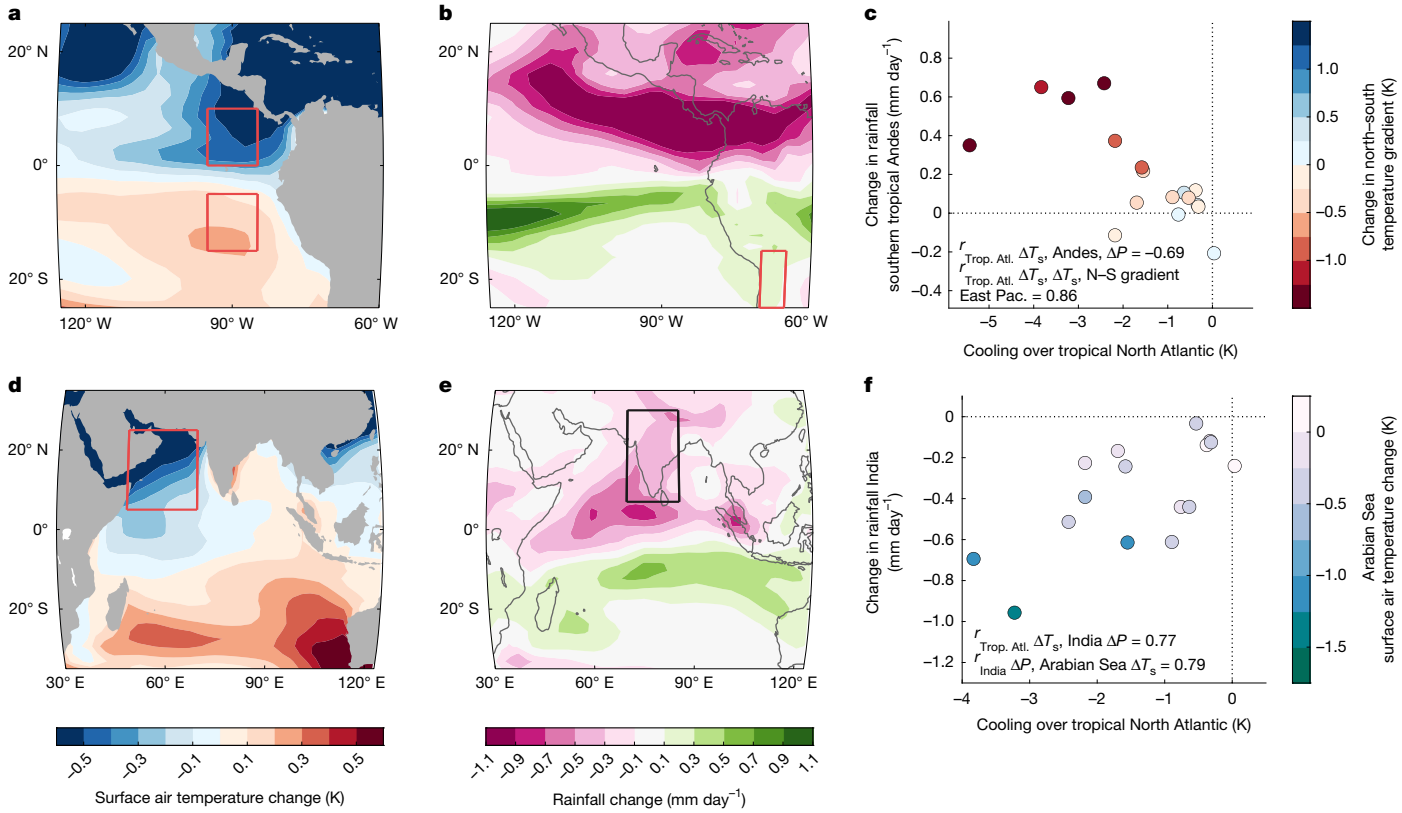

Fig. 4 | Simulated climate responses in the eastern tropical Pacific and the Indian Ocean. a,**b**,**d**,**e**, Changes in annual mean surface air temperature and rainfall averaged across simulations with moderate cooling in the tropical North Atlantic. **c**, Relationship between changes in the magnitude of the rainfall changes over the southern tropical Andes (70–65° W 25–15° S) (*y*-axis) and the magnitude of tropical Atlantic cooling as defined in the Methods (*x*-axis). Colours in each circle indicate the changes in the north–south surface air temperature gradient across the equator in the eastern Pacific, computed as the difference between the surface air temperature change north of the equator (95–85° W 0–10° N) minus south of the equator (85–80° W 10° S–0°). Negative values indicate a relaxation of the climatological north–south gradient. Each circle corresponds to a simulation in the full ensemble (Extended Data Table 1). **f**, Relationship between changes in rainfall over India (70–85° E 7–30° N) (*y*-axis) and the magnitude of tropical Atlantic cooling (*x*-axis). Colours in each circle indicate the magnitude of cooling over the Arabian Sea (50–70° E 5–25° N).

of the temperature and rainfall responses are important for capturing the palaeoclimatic evidence for wetter conditions over this region. Both the weakened temperature gradient across the equator and the increase in rainfall in the southern tropical Andes are highly correlated with the magnitude of temperature responses over the tropical Atlantic across simulations (Fig. 4c; $r = -0.69$ and $r = 0.86$, respectively). These changes involve a reduction in the climatological north–south temperature gradient and associated cross-equatorial winds in the eastern tropical Pacific[20,21]. The consistency between these responses in our ensemble, together with the palaeoclimatic evidence of the associated hydrological responses during HS1, demonstrates that this is the main pathway through which an AMOC collapse influences the Pacific Ocean, irrespective of the magnitude of high-latitude cooling.

In the Indian Ocean, the response resembles a southward shift in the ITCZ, although the underlying mechanisms causing this response are not directly associated with the Atlantic ITCZ shift. This is evident in the fact that all models show an Atlantic ITCZ response (Fig. 2), but only the models with moderate (and strong) cooling of the tropical Atlantic show the north–south precipitation dipole in the Indian Ocean that is evident in proxy data (Fig. 4e and Extended Data Fig. 7). The models suggest that cooling of the Arabian Sea is crucial to driving this response (Fig. 4d,e), and this response is enhanced when high-latitude cooling propagates over the subtropics and tropics in the North Atlantic. Colder Arabian sea-surface temperatures reduce the supply of moisture for the Indian monsoon, resulting in widespread drying over the northern Indian Ocean and south Asia (Fig. 4e). This mechanism is supported by the high correlation ($r = 0.79$; Extended Data Fig. 8) between the magnitude of the Arabian Sea cooling and the drying over India across simulations (Fig. 4f). In simulations with tropical Atlantic cooling, the cooling of the Arabian Sea also excites an inter-hemispheric temperature gradient in the Indian Ocean (Extended Data Fig. 7). This inter-hemispheric temperature dipole weakens the cross-equatorial trade winds (Extended Data Fig. 9) driving warming over the southeastern Indian Ocean (Fig. 4d). As a result, the weaker winds and warmer ocean temperatures increase the moisture convergence over northern Australia strengthening the austral summer monsoon (Fig. 4e and Extended Data Fig. 9). This response is consistent with palaeoclimatic evidence for wetter conditions in northern Australia during HS1. Further details on the mechanisms are available in the Supplementary Discussion.

Tropical North Atlantic cooling pattern

Our analysis demonstrates that cooling of the tropical Atlantic can effectively weaken the Indian monsoon, explaining one of the most conspicuous hydroclimatic responses during HS1. This influence occurs in an eastward direction as the westerly winds transport colder air generated in the subtropical North Atlantic across North Africa and the Arabian Peninsula[22,23]. The colder subtropical air ultimately cools the Arabian Sea triggering coupled ocean-atmosphere responses in the Indian Ocean (Fig. 4d). Other mechanisms could reinforce this eastward response[24–26], explaining some of the scatter among the simulated changes (Fig. 4f). Cooling of the Arabian Sea represents a pathway for a mid-latitude influence on the Indian monsoon bypassing the topographic insulation that characterizes this monsoon system[27].

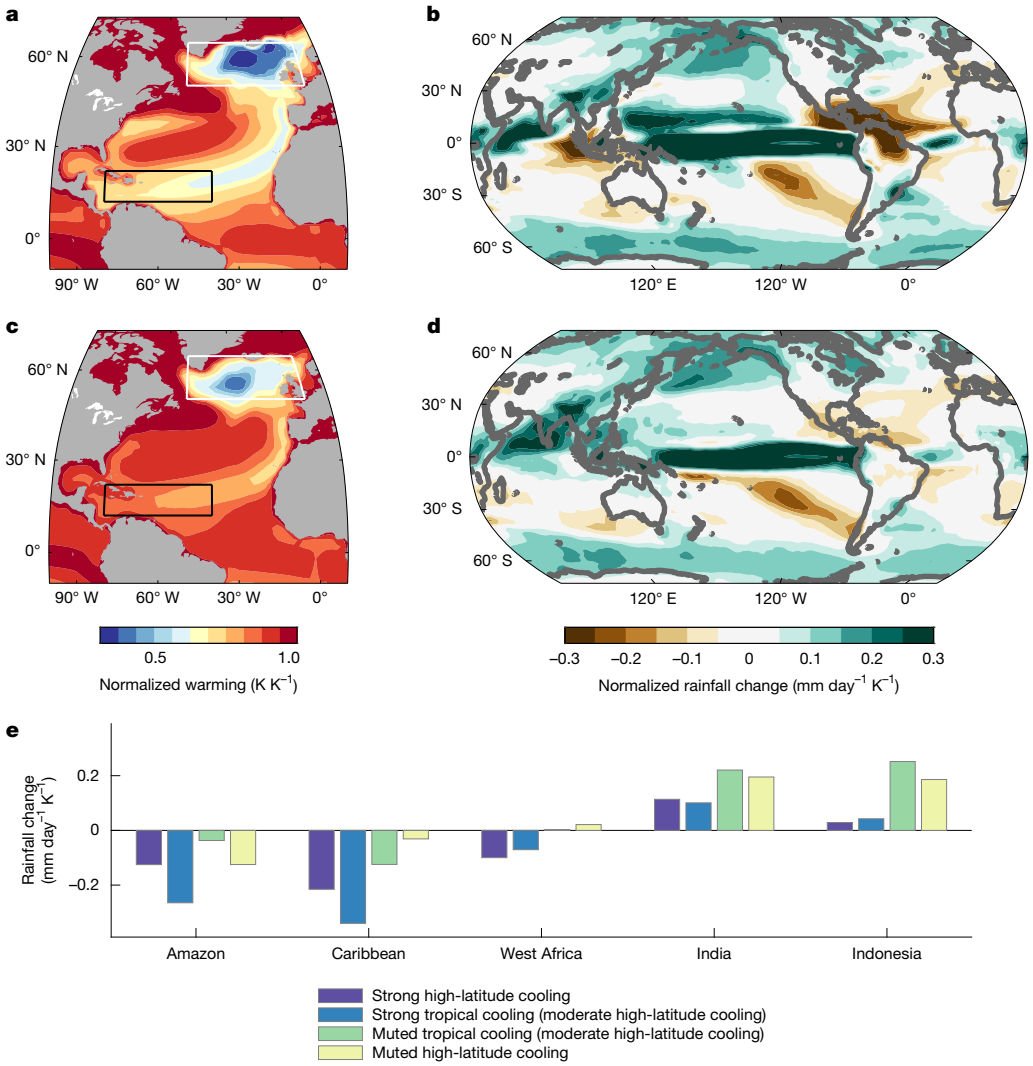

Fig. 5 | Surface temperature and rainfall changes in response to greenhouse warming associated with cooling patterns over the North Atlantic. **a**–**e**, Twenty-first century projections according to models with strong cooling over the tropical North Atlantic (**a**,**b**) compared with the models with cooling restricted to the high latitudes (**c**,**d**). **e**, Rainfall response averaged over key regions in which the tropical cooling pattern produces drying or a more muted rainfall increase. The high-emission projections used in the analysis were obtained from phases 3, 5 and 6 of the CMIP[36–38] as described in the Methods. The strong and muted tropical cooling responses are based on the magnitude of sea-surface temperature change over the tropical North Atlantic (80° W–40° W 12° N–22° N) relative to the surface temperature change over the tropics (30° S–30° N). The strong and muted high-latitude cooling responses are isolated based on the magnitude of sea-surface temperature change over the North Atlantic (60° W–0° 50° N–65° N) relative to the surface temperature change over the Northern Hemisphere (0°–90° N). Surface temperature and rainfall changes are computed for each individual model as the linear trend from 2021 to 2100, normalized by the magnitude of tropical mean surface warming over the same interval, and then composited based on the North Atlantic cooling responses described above.

This analysis shows that a westward influence by a weakened Pacific Walker circulation proposed by previous work[6,11] cannot explain the overwhelming evidence of wetter conditions over northern Australia nor is active in our ensemble, suggesting a state or model dependence.

Palaeo temperature records from the tropical Atlantic provide evidence of significant ocean cooling during HS1 in support of our results (Extended Data Fig. 6 and Supplementary Information section 3). However, most sites are located in the periphery of the simulated pattern, and potentially influenced by small-scale coastal processes not resolved by climate models[28], preventing an accurate evaluation of the magnitude of the temperature response. Regardless, most of the records show cooling (10 out of 13) with changes broadly consistent with the simulated pattern extending from the coast of Africa to the western Caribbean. Additional key patterns of ocean change involved in the global response are also supported by palaeodata, such as the weakened inter-hemispheric temperature gradient in the eastern Pacific[29] and the cooling of the Arabian Sea[30]. These patterns are essential to explain rainfall patterns in the Americas, along the eastern Pacific and across the Indian Ocean, and are properly simulated by models that simulate cooling over the tropical North Atlantic.

Multi-model projections

The differences in the tropical responses identified here suggest that a similar model dichotomy could occur in future simulations where anthropogenic warming leads to an AMOC slowdown or collapse[3,31]. To address this, we examined the tropical North Atlantic temperature response in available multi-model predictions used by the Intergovernmental Panel on Climate Change (IPCC). These global warming simulations show a wide range of AMOC responses to future warming, evidenced by the degree of cooling (or reduction in warming) over the high-latitude North Atlantic (Methods and Extended Data Fig. 10).

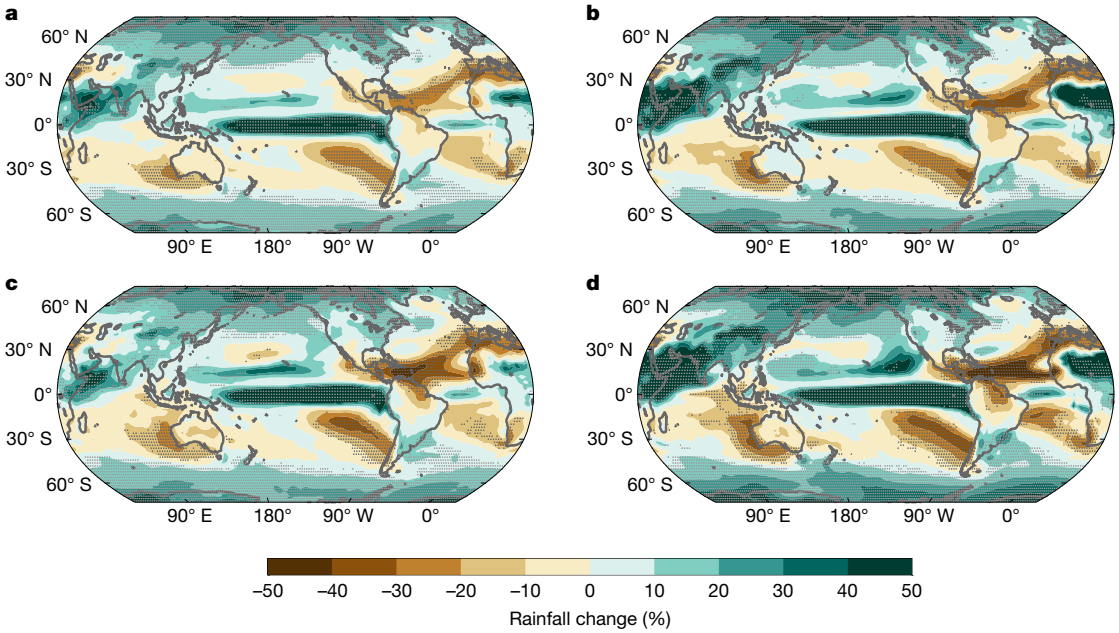

Fig. 6 | Impact of model validation on rainfall projections. a–d, Projected rainfall changes under high-emissions scenarios according to the AR5 and AR6 by the IPCC. Models participating in phases 5 and 6 of the CMIP[37,38] were used to reproduce the rainfall predictions in the AR5 (**a**,**c**) and AR6 (**b**,**d**), respectively. Rainfall changes are computed for each individual model as the annual mean change between the 2081–2100 and 1986–2005 periods and then averaged to produce the multi-model mean prediction. Stippling indicates regions in which 90% of models in each ensemble agree on the sign of the change following the criterion used by the IPCC in the AR5 (ref. 1). The number of models used to calculate the multi-model mean is indicated for each ensemble. Palaeo-validated models (**c**,**d**) are future simulations with a weakened AMOC collapse in which significant cooling extends into the tropical North Atlantic (defined as a relative warming of <0.8 K K^{-1} in that region), consistent with the tropical temperature response in palaeodata for an AMOC collapse.

Normalization of temperature responses relative to Northern Hemisphere and tropical means allows us to distinguish the patterns associated with AMOC weakening relative to other responses to greenhouse forcing, such as the well-known acceleration of the hydrological cycle[32]. To isolate differences in the tropical response, we focus our analysis on a subset of models (63 out of 77) with moderate AMOC-induced temperature responses in the North Atlantic defined by normalized warming over the high-latitude North Atlantic between 0 K K^{-1} and 1 K K^{-1} (Extended Data Fig. 10, upward and downward triangles, *y*-axis). The remaining 14 simulations are used to approximate the rainfall responses to very strong or muted high-latitude cooling (Fig. 5e, purple and yellow bars).

We find that despite the wide range of high-latitude temperature responses, the biggest influence on tropical rainfall occurs when models simulate AMOC-induced cooling reaching the western tropical North Atlantic and Caribbean Sea (Fig. 5a), similar to what we see in the HS1 freshwater hosing simulations. This subset of 25 models predicts pronounced drying over the Caribbean, Central America and northern South America and Amazon, as well as muted rainfall responses over the Maritime Continent and the Indian monsoon region, similar to the changes during HS1 (Fig. 5b). By contrast, the 38 models with similar high-latitude AMOC cooling, but a muted temperature response in the tropical Atlantic (Fig. 5c), simulate more muted tropical rainfall responses (Fig. 5d). The largest differences occur over the Amazon and the Caribbean (Fig. 5e, blue bars compared with green bars), although the tropical North Atlantic cooling effect also drives more muted rainfall changes over India and Indonesia (Fig. 5e, blue bars), opposing the tendency towards increasing rainfall driven by the thermodynamic increases in moisture driven by greenhouse warming (Fig. 5e, yellow bars). In many regions, for example, the Amazon, the Caribbean and India, the rainfall responses associated with tropical cooling are more pronounced or comparable to those in models with the strongest high-latitude cooling (Fig. 5e, purple bars compared with blue bars), highlighting the importance of sea-surface temperature changes in the tropical North Atlantic as amplifiers of the tropical influence of AMOC changes.

Reduced uncertainty by palaeo-evaluation

Our results show important details on the tropical response to AMOC collapse that are possible because of our new model evaluation against palaeoclimate data. Our model evaluation showed key features of the climate response to a weaker AMOC that are relevant for predicting future changes. First, cooling over the tropical North Atlantic, a response previously seen in single model simulations[4,6], is the main pathway through which an AMOC collapse influences the global tropics. Other mechanisms, such as the ITCZ shift, have limited regional influence. Second, models showing either a muted or excessive cooling response in the tropical Atlantic produce unrealistic changes in rainfall regardless of the size of the high-latitude temperature response and the magnitude of AMOC reduction, indicating that the differences in model response are not related to the magnitude of the forcing. This provides a way to reconcile the possibility that a more modest AMOC reduction during HS1[10] could explain the palaeoclimatic evidence of large changes in tropical hydroclimate. Conversely, it supports our conclusion that future AMOC reductions, even if they do not result in a full collapse, could have a large impact across the global tropics. Third, the broad range of cooling responses seen in models over the North Atlantic probably reflects the differences in model physics. The cooling pattern in the North Atlantic resembles the air–sea interactions involved in the wind–evaporation–SST feedback[33]. Thus, our results could reflect model differences in the strength or activation of this feedback. Given its importance connecting high and low latitudes, the model deficiencies identified here could lead to erroneous responses to other hemispheric forcings associated with tropical Atlantic temperatures, such as industrial aerosols, greenhouse gases or volcanic eruptions.

Changes in sea-surface temperatures over the tropical North Atlantic could thus play an important part in amplifying future changes in

rainfall across the tropics. This response is not simulated by all models used in the current climate assessments, indicating an error of importance for predicting future changes. We find that models that simulate a cooling pattern in agreement with past changes produce more reliable drought predictions over the Caribbean, Central America, the Amazon and West Africa. Over these regions, the Fifth and Sixth Assessment Reports (AR5 and AR6) by the IPCC showed highly uncertain rainfall changes (Fig. 6a,b). Note that areas with future drought show very little stippling, that is, low model agreement, consistent with Figure SPM.8 in the Summary for Policy Makers of the AR5 (ref. 1) and Cross-Chapter Box 11.1, Fig. 2 of Chapter 11 of the AR6 (ref. 2). We performed the same analysis, but selecting the models based on their ability to simulate the cooling pattern in the tropical North Atlantic. The resulting ensembles predict stronger drought than the consensus of models used by the IPCC, reaching a 40% reduction in rainfall over parts of the Amazon for AR6 models exhibiting the palaeo-validated response to AMOC collapse (Fig. 6d). Moreover, both ensembles of palaeo-validated AR5 and AR6 models show much higher agreement among the models, leading to more reliable predictions (Fig. 6c,d; note the increase in stippled areas with future drought). Therefore, cooling over the tropical Atlantic is more important for predicting rainfall responses across the tropics than the magnitude of the AMOC reduction itself or the associated hemispheric cooling. As such, future changes in tropical rainfall could also be significant, even if the predicted changes in AMOC strength during this century do not result in a full collapse as predicted by the models[34,35]. This heightened risk of future drought will fall on vulnerable societies and ecosystems across the tropics, particularly Central America, the Amazon and Indonesia, adding urgency to the mitigation of human emissions of greenhouse gases.

Online content

Any methods, additional references, Nature Portfolio reporting summaries, source data, extended data, supplementary information, acknowledgements, peer review information; details of author contributions and competing interests; and statements of data and code availability are available at https://doi.org/10.1038/s41586-025-09319-x.

1. Intergovernmental Panel on Climate Change in *Climate Change 2013: The Physical Science Basis: Working Group I Contribution to the Fifth Assessment Report of the Intergovernmental Panel on Climate Change* (eds Stocker, T. F. et al.) 1–30 (Cambridge Univ. Press, 2013).
2. Seneviratne, S. I. et al. in *Climate Change 2021: The Physical Science Basis: Working Group I Contribution to the Sixth Assessment Report of the Intergovernmental Panel on Climate Change* (eds Masson-Delmotte, V. et al.) 1513–1766 (Cambridge Univ. Press, 2021).
3. Bellomo, K., Angeloni, M., Corti, S. & von Hardenberg, J. Future climate change shaped by inter-model differences in Atlantic meridional overturning circulation response. *Nat. Commun.* **12**, 3659 (2021).
4. Dong, B.-W. & Sutton, R. T. Adjustment of the coupled ocean-atmosphere system to a sudden change in the Thermohaline Circulation. *Geophys. Res. Lett.* **29**, 18-1–18-4 (2002).
5. Vellinga, M. & Wood, R. A. Global climatic impacts of a collapse of the Atlantic thermohaline circulation. *Clim. Change* **54**, 251–267 (2002).
6. Zhang, R. & Delworth, T. L. Simulated tropical response to a substantial weakening of the Atlantic thermohaline circulation. *J. Clim.* **18**, 1853–1860 (2005).
7. Kang, S. M., Held, I. M., Frierson, D. M. W. & Zhao, M. The response of the ITCZ to extratropical thermal forcing: idealized slab-ocean experiments with a GCM. *J. Clim.* **21**, 3521–3532 (2008).
8. Kageyama, M. et al. Climatic impacts of fresh water hosing under Last Glacial Maximum conditions: a multi-model study. *Clim. Past.* **9**, 935–953 (2013).
9. Lynch-Stieglitz, J. The Atlantic meridional overturning circulation and abrupt climate change. *Annu. Rev. Mar. Sci.* **9**, 83–104 (2017).
10. Pöppelmeier, F., Jeltsch-Thömmes, A., Lippold, J., Joos, F. & Stocker, T. F. Multi-proxy constraints on Atlantic circulation dynamics since the last ice age. *Nat. Geosci.* **16**, 349–356 (2023).
11. Clement, A. C. & Peterson, I. C. Mechanisms of abrupt climate change of the last glacial period. *Rev. Geophys.* **46**, RG4002 (2008).
12. Orihuela-Pinto, B., England, M. H. & Taschetto, A. S. Interbasin and interhemispheric impacts of a collapsed Atlantic Overturning Circulation. *Nat. Clim. Change* **12**, 558–565 (2022).
13. Smeed, D. A. et al. The North Atlantic Ocean is in a state of reduced overturning. *Geophys. Res. Lett.* **45**, 1527–1533 (2018).
14. Boers, N. Observation-based early-warning signals for a collapse of the Atlantic Meridional Overturning Circulation. *Nat. Clim. Change* **11**, 680–688 (2021).
15. Kilbourne, K. H. et al. Atlantic circulation change still uncertain. *Nat. Geosci.* **15**, 165–167 (2022).
16. McManus, J. F., Francois, R., Gherardi, J.-M., Keigwin, L. D. & Brown-Leger, S. Collapse and rapid resumption of Atlantic meridional circulation linked to deglacial climate changes. *Nature* **428**, 834–837 (2004).
17. Stager, J. C., Ryves, D. B., Chase, B. M. & Pausata, F. S. R. Catastrophic drought in the Afro-Asian monsoon region during Heinrich event 1. *Science* **331**, 1299–1302 (2011).
18. Andrews, J. T. & Voelker, A. H. "Heinrich events" (& sediments): a history of terminology and recommendations for future usage. *Quat. Sci. Rev.* **187**, 31–40 (2018).
19. DiNezio, P. N. & Tierney, J. E. The effect of sea level on glacial Indo-Pacific climate. *Nat. Geosci.* **6**, 485–491 (2013).
20. Timmermann, A. et al. The influence of a weakening of the Atlantic meridional overturning circulation on ENSO. *J. Clim.* **20**, 4899–4919 (2007).
21. Xie, S.-P., Okumura, Y., Miyama, T. & Timmermann, A. Influences of Atlantic climate change on the tropical Pacific via the Central American isthmus. *J. Clim.* **21**, 3914–3928 (2008).
22. Liu, Y., Chiang, J. C. H., Chou, C. & Patricola, C. M. Atmospheric teleconnection mechanisms of extratropical North Atlantic SST influence on Sahel rainfall. *Clim. Dyn.* **43**, 2797–2811 (2014).
23. DiNezio, P. N. et al. Glacial changes in tropical climate amplified by the Indian Ocean. *Sci. Adv.* **4**, eaat9658 (2018).
24. Marzin, C., Kallel, N., Kageyama, M., Duplessy, J.-C. & Braconnot, P. Glacial fluctuations of the Indian monsoon and their relationship with North Atlantic climate: new data and modelling experiments. *Clim. Past* **9**, 2135–2151 (2013).
25. Otto-Bliesner, B. L. et al. Coherent changes of southeastern equatorial and northern African rainfall during the last deglaciation. *Science* **346**, 1223–1227 (2014).
26. Mohtadi, M. et al. North Atlantic forcing of tropical Indian Ocean climate. *Nature* **509**, 76–80 (2014).
27. Boos, W. R. & Kuang, Z. Dominant control of the South Asian monsoon by orographic insulation versus plateau heating. *Nature* **463**, 218–222 (2010).
28. Wan, X., Chang, P., Saravanan, R., Zhang, R. & Schmidt, M. W. On the interpretation of Caribbean paleo-temperature reconstructions during the Younger Dryas. *Geophys. Res. Lett.* **36**, L02701 (2009).
29. Kienast, M. et al. Eastern Pacific cooling and Atlantic overturning circulation during the last deglaciation. *Nature* **443**, 846–849 (2006).
30. Tierney, J. E., Pausata, F. S. R. & deMenocal, P. Deglacial indian monsoon failure and North Atlantic stadials linked by indian ocean surface cooling. *Nat. Geosci.* **9**, 46–50 (2016).
31. Liu, W., Xie, S.-P., Liu, Z. & Zhu, J. Overlooked possibility of a collapsed Atlantic meridional overturning circulation in warming climate. *Sci. Adv.* **3**, e1601666 (2017).
32. Held, I. M. & Soden, B. J. Robust responses of the hydrological cycle to global warming. *J. Clim.* **19**, 5686–5699 (2006).
33. Xie, S.-P. & Philander, G. H. A coupled ocean-atmosphere model of relevance to the ITCZ in the eastern Pacific. *Tellus A* **46**, 340–350 (1994).
34. Gregory, J. M. et al. A model intercomparison of changes in the Atlantic thermohaline circulation in response to increasing atmospheric CO_2 concentration. *Geophys. Res. Lett.* **32**, L12703 (2005).
35. Weijer, W., Cheng, W., Garuba, O. A., Hu, A. & Nadiga, B. T. CMIP6 models predict significant 21st century decline of the Atlantic meridional overturning circulation. *Geophys. Res. Lett.* **47**, e2019GL086075 (2020).
36. Meehl, G. A. et al. THE WCRP CMIP3 multimodel dataset: a new era in climate change research. *Bull. Am. Meteorol. Soc.* **88**, 1383–1394 (2007).
37. Taylor, K. E., Stouffer, R. J. & Meehl, G. A. An overview of CMIP5 and the experiment design. *Bull. Am. Meteorol. Soc.* **93**, 485–498 (2012).
38. Eyring, V. et al. Overview of the Coupled Model Intercomparison Project Phase 6 (CMIP6) experimental design and organization. *Geosci. Model Dev.* **9**, 1937–1958 (2016).

Methods

Ensemble of freshwater hosing simulations

Our main dataset is an ensemble of 17 simulations of global climate in which the strength of the AMOC is weakened by applying a flux of freshwater over the high-latitude North Atlantic. This approach of simulating an AMOC collapse, generally referred to as freshwater hosing, has been extensively applied in climate models[5,6,39,40] to circumvent limitations in the representation of physical processes that trigger Heinrich events, such as ice sheet instability, iceberg discharge and the distribution and propagation of a freshwater anomaly over the ocean surface. All simulations implemented the freshwater flux as a spatially uniform negative salinity flux over the North Atlantic, particularly over areas of wintertime convection in the Labrador and Greenland seas. The magnitude of this flux ranged from 0.1 Sv to 0.2 Sv (1 Sv = 10^6 m^3 s^{-1}) in most simulations, consistent with the record of sea-level rise during Heinrich events[41,42]. Two simulations used much higher values (0.4 Sv and 1 Sv) to consider extreme AMOC responses in the ensemble. The freshwater flux was applied over different regions over the North Atlantic, including the Ruddiman Belt (40°–50° N)—in which palaeoclimatic evidence shows the effect of iceberg discharge, the mid- to high-latitude North Atlantic (50°–70°) and the Greenland–Iceland–Norwegian Seas (GIN, north of about 65°N in the Atlantic). Nine simulations are part of an existing ensemble[40], which we augmented with eight simulations using newer models or existing models forced with different rates of freshwater (Extended Data Table 1).

All hosing simulations were run relative to glacial background conditions to perform a more realistic evaluation because the rainfall responses to AMOC reductions will depend on the location of climatological rainfall patterns under glacial conditions. It is also important to consider the influence of initial oceanic states, particularly the strength of the AMOC, which shows a wide range of magnitudes, from 8.4 Sv to 26.8 Sv in our simulations. Simulations performed with the MIROC (Model for Interdisciplinary Research on Climate) and COSMOS are particularly useful to assess the sensitivities to the strength of the glacial AMOC. Two of these simulations were run relative to glacial states with a strong AMOC (MIROC-S and COSMOS-S)—typical of glacial simulations[43]— whereas the remaining two simulations have a weak glacial AMOC (MIROC-W and COSMOS-W)—consistent with palaeoclimatic evidence[16]. These simulations helped us explore the sensitivity of the model-proxy agreement to the initial AMOC state.

Several simulations were run with the same model with freshwater forcing applied at different locations or rates. Simulations performed with HadCM3 were run under low and high rates of freshwater forcing (HadCM3-0.1Sv and HadCM3-0.4Sv). These two simulations used glacial boundary conditions for 24,000 years before present (ka BP) (ref. 44). The rest of the models used 21 ka BP boundary conditions corresponding to the LGM following versions 2 or 3 of the PMIP protocol[45,46]. More details on their implementation can be found in their original publications listed in Extended Data Table 1. The existing ensemble[8] included two simulations performed with the CCSM3 developed at the National Center for Atmospheric Research (NCAR) in which freshwater fluxes were applied in different regions of the North Atlantic: 0.1 Sv applied over the North Atlantic (CCSM3-0.1Sv-NA) and 0.2 Sv applied to the Greenland, Iceland and Norwegian seas (CCSM3-0.2Sv-GIN-LR).

We expanded the ensemble with three additional simulations performed with CCSM3 to explore the impact of resolution and freshwater rates. In CCSM3-0.2Sv-GIN-HR, the model was configured with higher atmospheric and oceanic resolution (T85 1.4° and 1°, respectively) and forced with 0.2 Sv applied over the GIN seas[47]. This simulation was run for 400 years with climatologies computed from the past 50 years. The LGM control followed the PMIP2 protocol[48]. In CCSM3-1Sv, the model was configured at T42 atmospheric resolution (2.8°) and 1° ocean resolution and was forced with the extreme rate of 1 Sv over the North Atlantic (50°–70°) (ref. 49). The climatologies are based on 100-year averages of equilibrated climate. We also included output from the TraCE-21ka experiment[41], performed with the lower resolution version of the CCSM3 model (T31 atmosphere/3° ocean), but forced solely by a time-varying melt water flux (CCSM3-TraCE-MWF), with other external forcings (for example, insolation, ice sheet and greenhouse gases) held constant at LGM levels. This is a transient simulation in which the freshwater flux increases gradually during 19–17 ka, then stays constant during 17–15 ka with the equivalent magnitude of 0.17 Sv (ref. 50). The background climate was obtained by averaging between years 19,000 and 21,000, and the interval with reduced AMOC between years 15,000 and 17,000. The four simulations performed with CCSM3 used different model resolutions, allowing the study of the sensitivity of the results to model resolution and rates, and location of freshwater forcing.

Our ensemble includes five new, unpublished simulations performed with more recent versions of the IPSL and NCAR models. A new simulation was performed with the IPSL-CM5 forced with 0.1 Sv applied over the North Atlantic (50°–70° N). This simulation was run for 400 years with the climatology obtained from the past 300 years of equilibrated climate. The control climatology was based on 300 years of equilibrated LGM climate. We also included a new simulation performed with v.1.2.2 of the NCAR Community Earth System Model (CESM) configured with CAM4 atmospheric physics and land carbon-nitrogen cycling. This simulation was forced with 0.1 Sv applied over the Ruddiman Belt (North Atlantic, 40°–50° N) for 200 years. We label this simulation CCSM4-0.1Sv-RB because the use of CAM4 physics makes this model configuration closer to its previous version, CCSM4. This simulation and its LGM control used the GLAC-1D ice sheet reconstruction[51], unlike the rest of the simulations, which followed the PMIP2 or PMIP3 protocols. The past 30 years of each simulation were used to compute the climatologies used in the analysis. We complete the ensemble with three new simulations performed with v.1.2.1 of the CESM1 configured with CAM5 atmospheric physics under different magnitudes of freshwater hosing (0.1 Sv, 0.15 Sv and 0.2 Sv) applied over the North Atlantic (50°–70° N). These simulations are based on an existing LGM simulation performed following the PMIP3 protocol[23]. All three hosing simulations were run for 200 years, with the past 50 years used to compute the climatologies used in the analysis. Further details on the ensemble are provided in Supplementary Information section 1.

The simulated patterns of rainfall change are broadly consistent among the 17 hosing simulations analysed here (Extended Data Fig. 2). The models simulate drier conditions in the northern tropics and wetter conditions in the southern tropics—a pattern broadly consistent with a southward shift in the ITCZ associated with the cooling of the North Atlantic. The hosing simulations, such as the palaeoclimate proxies, exhibit large departures from this global pattern at the regional level, particularly over land, where monsoonal responses may not be directly driven by the global shift in the ITCZ[52,53]. Furthermore, the rainfall patterns are most consistent among models in the circum-Atlantic region, less consistent in the eastern Pacific and eastern Africa, and rather inconsistent in the western Pacific and over the Maritime Continent. For instance, all hosing simulations, except CESM1-0.1Sv-NA, show drier conditions over the northwestern coast of Africa, the Indian Ocean and the Indian subcontinent. Most of the simulations show wetter conditions in southern Africa and northeastern Brazil. However, the sign of the rainfall response (wet and dry) over the Pacific Ocean, across the Maritime Continent and over much of South America and East Asia is not consistent among most simulations.

Synthesis of hydroclimate changes during HS1

Our synthesis of hydroclimate changes during HS1 is based on a collection of 220 published records based on rainfall-sensitive proxies. The collection was last updated in August 2024 with recently published records. Our evaluation of model responses is based on a subset of 125 records selected based on their location, resolution, length and co-location with the climate signal. The abundance of records allowed

us to robustly reconstruct patterns of change across the global tropics, which combined with the availability of multi-model hosing simulations, motivates our focus on HS1 relative to other intervals with evidence of AMOC reductions, such as the Younger Dryas or the 8.2 ka events. We did not study the Younger Dryas event because of the limited availability of multi-model simulations for this interval. Conversely, there are not enough records with the temporal resolution required to resolve the much shorter 8.2 ka event, preventing us from reconstructing spatial patterns of change with the level of detail as for HS1.

All records are based on proxies explicitly defined as sensitive to hydroclimate changes by their original authors. Records were categorized according to the following proxy types: terrestrial isotope, aridity or vegetation, allowing us to explore the sensitivity of the model-proxy agreement. Terrestrial isotope records include hydrogen isotope ratios from leaf waxes (δD_{wax}) from both marine and lacustrine sediment, oxygen isotope ratios from cave speleothems ($\delta^{18}O_{calcite}$) and hydrogen isotope ratios from ice cores from tropical glaciers (δD_{ice}). Aridity records include dust flux, terrigenous discharge (for example, titanium or aluminium fluxes) and high-resolution lake-level reconstructions. Vegetation records encompass carbon isotope ratios ($\delta^{13}C$) and pollen records from marine or lacustrine sediments. Marine isotope records, including $\delta^{18}O$ of seawater, were not included because sea-surface salinity fields were not available for direct model-proxy comparison. Three isotope records from ice cores from the tropical Andes[54–56] were excluded because of a lack of consensus in the literature on whether they capture hydroclimate or temperature changes. Excluding these records did not affect our results because multiple nearby records supported the pattern of wet conditions in both the Timor Sea and the tropical Andes.

The domain used for record selection spans the global tropics (25° S–25° N). In Central America, this boundary was extended to 30° N to include a site in northern Mexico potentially sensitive to changes in the North American monsoon[57]. Similarly, records as far north as 35° were included along the coast of North Africa, where there could be a direct influence of changes related to the West African monsoon. Several stalagmite $\delta^{18}O$ records from China north of 25° N were excluded because they may reflect non-local effects[58], and therefore it is unclear whether they should be compared against local rainfall changes. However, the results are not sensitive to this choice because these records consistently show a drier HS1 in agreement with the simulations with moderate tropical North Atlantic cooling (Fig. 2a). Over India, we extended the domain northwards to include Bittoo Cave at about 30° N in the Himalayas, where there is evidence of local hydroclimate changes associated with the Indian summer monsoon[59]. We also extended the domain over South America to 28° S to include records that have been associated with monsoonal changes[60,61].

Record selection focused on temporal resolution and length to resolve changes during HS1 and to define the glacial or deglacial baseline before the onset of HS1, respectively. Record resolution was required to be at least about 500 years during the 17.5–5 ka interval for HS1. Considering potential age uncertainties, analytical errors and varying signal-to-noise ratios, this requires at least 5 data points between 17.5 ka and 15 ka. This criterion was important to exclude records that cannot reliably resolve a change during HS1. Mainly, it avoids aliasing climate or proxy noise into a millennial-scale signal that could be confounded as a response to changes in the North Atlantic climate during HS1. Although it led to the exclusion of many records, this criterion was particularly important to identify those few, important locations with robust evidence of negligible changes for our 'unchanged' category. These sites were essential to delineate the spatial extent of patterns of drying or wetting. A record length extending back to the LGM (21–19 ka BP) was required to ensure that a change during HS1 can be robustly defined relative to a well-defined baseline climate. Alternatively, if the record was shorter, we required a clear deglacial trend to define the changes. For instance, previous work focusing on tropical changes[17] inferred changes relative to a Holocene baseline—sometimes using records without a clearly defined glacial state.

A total of 125 records meeting the selection criteria (proxy type, tropical domain, record resolution, length and co-location with climate signal) were used for pattern evaluation of the models. These records were selected out of 157 records included in our published database, from which we excluded 29 marine isotopic records measuring $\delta^{18}O$ of seawater and three records based on vegetation proxies without a clear link to a co-located pattern of climate change. For each selected record, the changes during HS1 were categorized as wetter, unchanged or drier relative to the glacial or deglacial baseline. Most of the records (102) were categorized following the original published interpretation. The remaining subset of records (23) required reinterpretation. This was done after multiple inspections of the records by many members of our team to ensure robust results. Most of these records (17) required reinterpretation because the original authors did not identify a change during HS1. We categorized many of these records (8) as unchanged, potentially explaining why the original authors did not report a change during HS1. The rest of the records (9) show a clear dry or wet HS1 anomaly. A small subset of records (6) required us to change the original interpretation because of either an unclear anomaly (4) or an unclear baseline (2). Further details are provided in Supplementary Information section 2 and with the published synthesis[62].

Most of the selected records have chronologies based on radiocarbon or U–Th dating (117 out of 125), and fewer records (8 records) have chronologies based on less accurate methods, such as correlations with paired records or optically stimulated luminescence. Although we did not use chronology as a limiting constraint on the choice of records, most of the records have sufficient chronological constraints to allow HS1 to be identified. Most of the records with U–Th or ^{14}C dates (111 out of 118) have at least three dates between the 10–21 ka BP interval. Only six records have two or fewer dates. The additional eight records had age models based on marine $\delta^{18}O$ stratigraphy (7) or optically stimulated luminescence (1). Further details are provided with the published synthesis[62].

The hydroclimate changes inferred from terrigenous discharge and dust records were located at the sites despite the non-local nature of the changes captured by these proxies. Most of the sites were located near the catchment or dust source and are in locations where large-scale patterns were simulated by the models. Records from sites within a radius of 100 km were merged, and the changes were labelled as not robust if the categorical changes did not agree for similar proxy types. This resulted in six merged sites, reducing the number of sites or records to 113. Merged sites are shown with larger triangles in all figures. Only one merged site included disagreeing records, and southern Africa was not included in the model evaluation.

Pattern agreement

We evaluated the responses in the models against proxy-inferred patterns following previous work[19]. This technique compares proxy-inferred changes in dry, unchanged and wet categories with simulated rainfall changes converted to the same categories. First, we compute the rainfall change as the difference in the annual mean precipitation (large-scale plus convective) between each HS1 hosing simulation minus its LGM control. Although some palaeoclimate records in our synthesis might be biased towards a specific season, for simplicity, we used simulated the annual mean responses in the evaluation. We normalize the rainfall change relative to the annual mean rainfall in the LGM control to ensure comparable values across regions with different hydrological regimes. We use rainfall as the main hydrological variable for comparison against proxy-inferred changes following the original methodology[19]. Although proxies are influenced by various processes, such as evaporation, extreme rainfall, atmospheric circulation or soil moisture, the sign of the change, that is, the dry, unchanged or wet categories, will be dominated by the rainfall changes in most of the proxies

in our synthesis, because typically these variables will change coherently. To conclude, we interpolated the normalized rainfall change to the location of each site for further comparison.

The merged sites that do not show a robust response are excluded from the κ calculation. Thresholds ranging from 1% to 100% are used to categorize the simulated in situ normalized rainfall changes into the wetter, drier or unchanged categories. Last, the κ statistic was computed between the simulated and the proxy-inferred in situ changes as a function of the threshold used to categorize the simulated changes. The κ statistic estimates the fractional agreement between the associated patterns relative to the probability of random agreement. It can range from 1, for perfect agreement, to 0, for no agreement. This categorical approach facilitates direct evaluation of the simulated patterns against the spatial patterns in the proxy data, avoiding the challenges of converting indirect proxy indicators into absolute rainfall amounts. This procedure generates a range of κ values as a function of the threshold used to categorize the model responses[19]. Throughout this study, we used the maximum κ for thresholds larger than 5% to quantify the best agreement between a simulated response and the proxy-inferred changes (for example, Figs. 1b or 3a,c).

Evaluation of regional responses

The simulated annual mean rainfall responses were grouped into strong, moderate and muted cooling (Extended Data Table 1), based on the magnitude of this response over the tropical North Atlantic (80–40° W 12–22° N). The cutoff values for grouping the simulations (−3 K and −1 K) define three distinct groups of responses. However, some simulations classified as muted showed a substantial degree of cooling, for example, CCSM4-1Sv-RB, but not as strong as the simulations in the moderate and strong groups (Extended Data Table 1). Ensemble averaging across simulations with cooling patterns of similar magnitude produces distinct levels of agreement (Fig. 3a). Ensemble averaging also produces rainfall responses across the tropics with distinct spatial patterns (Fig. 2). The magnitude of the cooling pattern in the tropical North Atlantic was quantified using air surface temperature because only this variable was available from all the models. Although air temperature is not exactly equal to sea-surface temperature, the changes over the tropical North Atlantic differ by less than 0.1 K in the CESM1 simulations that have both variables available. The rainfall changes associated with strong, moderate and muted cooling were isolated by averaging changes across simulations in each group. Ensemble averaging reduces the impact of different model formulations or background glacial climate, isolating the influence of the distinct cooling patterns.

We used the κ metric to evaluate regional responses associated with cooling patterns over the North Atlantic. The regions for this analysis were selected based on mechanisms proposed in the literature[8] as well as the availability of sites to resolve their spatial signature. Their extent was optimized to include a sufficient number of sites and produce statistically significant κ ($P < 0.05$), while making sure that we cover the global tropics. The 'East African, Indian and Australian monsoons' domain includes multiple responses because the patterns associated with individual monsoon systems could not be isolated with the available palaeoclimate records. However, we find that all the responses in this domain are ultimately related by the magnitude of cooling over the Arabian Sea, thus justifying the use of a larger, integrated domain. We exclude records from locations influenced by mid-latitude (not tropical) dynamics because they would not help us distinguish mechanisms communicating the response to the global tropics. The regions used to evaluate mechanisms are given below.

Atlantic ITCZ. Shifts in the Atlantic ITCZ were evaluated, focusing on sites in tropical South America and Africa (Fig. 3b, triangles). This domain includes West Africa, where the homonymous monsoon system could be driven by ventilation of colder, drier high-latitude air without a direct influence from the tropical Atlantic[22]. We do not separate this region from the larger tropical Atlantic domain because the available data do not allow us to estimate statistically significant κ values ($P < 0.05$). This domain excludes sites surrounding the Western Caribbean and Central America, which can also be affected by shifts in the Atlantic ITCZ, but they are more directly involved in the bridge mechanism to the eastern Pacific (see next region). Therefore, these sites are included in the 'Caribbean and Eastern Pacific ITCZ' domain because rainfall over those regions is more directly influenced by cooling over the Caribbean Sea, which we show is the mechanism communicating the response to the Pacific.

Caribbean and eastern Pacific ITCZ. Shifts in the eastern Pacific ITCZ were evaluated by focusing on sites from areas of Central America and along the west coast of tropical South America (Fig. 3d, triangles). This domain includes sites in the Caribbean and northern Central America, as well as modern-day Florida, that could be influenced by patterns of cooling over the Caribbean Sea.

Pacific Walker circulation. This domain includes sites in the Maritime Continent and along the west coast of South America, south of the equator (Fig. 3e). Simulated changes in rainfall over the sites in the Maritime Continent are not influenced by changes in the Indian Ocean and show responses associated with changes in the Pacific Walker circulation. The sites along the west coast of South America also capture rainfall changes associated with meridional shifts in the ITCZ. However, we also include them in this domain because they also reflect the changes in the Walker circulation.

East African, Indian and Australian monsoons. This domain focuses on sites in land areas surrounding the Indian Ocean, where rainfall variability is governed by these monsoon systems (Fig. 3f). This domain includes sites off the coast of Sumatra and Southeast Asia, where the simulated changes in rainfall are associated with changes in the Indian Ocean with a minimal influence from the Pacific Ocean.

Temperature and rainfall responses in global warming simulations

We used climate model simulations performed under high-emission scenarios to study the influence of future reductions in AMOC strength on tropical rainfall. Using high-emission scenarios allowed us to compare results between the AR5 and AR6. Both assessments showed that models disagree in the sign of the projected rainfall change under high-emission scenarios[1,2]. Projections are dominated by internal variability under low-emission scenarios that humanity is likely to exceed; therefore, we do not consider them in our analysis. A total of 77 simulations run with different models participating in phases 3, 5 and 6 of the CMIP were analysed. Eight simulations are from phase 3 (CMIP3) (ref. 36) performed following the SRES A2 scenario, 40 from phase 5 (CMIP5) (ref. 37) following the RCP8.5 scenario, and 29 from phase 6 (CMIP6) (ref. 38) following the SSP5–8.5 scenario. For each simulation, the change in sea-surface temperature or rainfall was computed based on least-squares linear trends over the 2021 to 2100 interval. Unlike the HS1 hosing simulations, these simulations show AMOC-induced cooling over the North Atlantic superimposed on the overall warming trend driven by increasing greenhouse gas concentrations. We isolated the cooling patterns associated with reductions in AMOC strength following previous work showing a high correlation between these responses in models[3]. The temperature change simulated by each model needs to be normalized to separate it from the global-warming-driven greenhouse forcing.

The intensity of AMOC-induced cooling is quantified as the sea-surface temperature change over the North Atlantic (50° W–0° 50° N–65° N) relative to the surface temperature change over the Northern Hemisphere (0°–90° N, both land and ocean). Similar results are obtained if the global mean is used in this normalization[3] or the tropical

mean, which we use in Fig. 5 to highlight patterns in the tropical North Atlantic. Most models show a normalized temperature response less than 1, indicative of AMOC-induced cooling (Extended Data Fig. 10, *x*-axis). Several models show negative values, indicative of absolute cooling, and very few models show values close to 1, indicative of muted cooling over the high-latitude North Atlantic. Using this metric to quantify the AMOC response allowed us to maximize the size of our ensemble because few modelling centres supplied the ocean overturning stream function to estimate AMOC strength directly. Similarly, we estimate the magnitude of the cooling response in the tropical North Atlantic as the simulated sea-surface temperature change over the tropical North Atlantic (80° W–40° W 12° N–22° N) relative to the surface temperature change over the tropics (30° S–30° N, both land and ocean). A normalized temperature change less than 1 indicates high-latitude cooling influencing the tropical North Atlantic, and conversely, values close to 1 indicate a muted influence of AMOC reduction cooling the tropical North Atlantic.

The global warming simulations show a wide range of warming rates in the high-latitude and tropical North Atlantic, suggesting a diversity of AMOC-induced responses (Extended Data Fig. 10). These cooling responses are not highly correlated ($r = 0.36$), suggesting that the two patterns are largely independent and therefore separable. To isolate the effect of these patterns on tropical rainfall, we classified the simulations into four different categories based on the magnitude of the relative warming in the high latitude and tropical North Atlantic. Most of the simulations (63 out of 77) show normalized warming over the high-latitude North Atlantic between 0 K $K^{-1}$and 1 K K^{-1} (Extended Data Fig. 10, upward-pointing and downward-pointing triangles), suggesting a degree of AMOC-induced cooling in this region relative to the hemispheric warming driven by greenhouse gas forcing. This subset of simulations shows a wide range of warming rates over the tropical North Atlantic (Extended Data Fig. 10, *y*-axis). We focused our analysis on these models because they have high-latitude temperature responses of comparable magnitude. Then we separated these 63 models into two additional subgroups based on whether the magnitude of tropical warming is smaller or larger than 0.8 K K^{-1} (Extended Data Fig. 10, upward-pointing and downward-pointing triangles, respectively). These two subgroups were used to isolate the rainfall responses to strong and muted tropical cooling shown in Fig. 5. Focusing our analysis on these two subsets of simulations allows us to isolate the effect of tropical cooling independently of the magnitude of high-latitude cooling, which is quite homogeneous among these 63 simulations. A small subset of the simulations (10 out of 77) show normalized cooling smaller than 0 K K^{-1} (that is, negative), suggesting much stronger AMOC-induced cooling (Extended Data Fig. 10, squares). Most of these simulations show a negative response, that is, absolute cooling (Extended Data Fig. 10, *x*-axis). These simulations are used to isolate the rainfall responses to strong high-latitude cooling (Fig. 4e, purple bars). Conversely, there is a subset of simulations (4 out of 77) with normalized warming larger than 1 K K^{-1}, that is, very weak high-latitude AMOC-induced cooling. These simulations are used to isolate the rainfall responses to muted high-latitude cooling (Fig. 4e, yellow bars). The changes in this subset of simulations approximate the tropical response to processes such as the wet-get-wetter and weaker Walker circulation[32,63], which in some places, for example, the tropical Pacific, can be much larger than the effect of AMOC reductions (not shown). Last, we normalized the magnitude of rainfall changes by the magnitude of tropical (30° N–30° S) surface warming (land and ocean) in each simulation before compositing them. This seeks to homogenize the responses of models with different rates of global warming.

Data availability

Our synthesis of hydroclimate changes during HS1 (ref. 62), including metadata, methods and references, is available at Zenodo[62] (https://doi.org/10.5281/zenodo.13881535). The original published records are available in published repositories as detailed by the individual publications listed in the document accompanying the synthesis.

Code availability

The MATLAB code used to perform the quantitative model-proxy evaluation and create the figures is available at Zenodo[79] (https://doi.org/10.5281/zenodo.13886977).

39. Manabe, S. & Stouffer, R. J. Simulation of abrupt climate change induced by freshwater input to the North Atlantic Ocean. *Nature* **378**, 165 (1995).
40. Kageyama, M. et al. Glacial climate sensitivity to different states of the Atlantic Meridional overturning circulation: results from the IPSL model. *Clim. Past* **5**, 551–570 (2009).
41. Liu, Z. et al. Transient simulation of last deglaciation with a new mechanism for bølling-allerød warming. *Science* **325**, 310–314 (2009).
42. Zhou, Y. & McManus, J. F. Heinrich event ice discharge and the fate of the Atlantic Meridional Overturning Circulation. *Science* **384**, 983–986 (2024).
43. Otto-Bliesner, B. L. et al. Last Glacial Maximum ocean thermohaline circulation: PMIP2 model intercomparisons and data constraints. *Geophys. Res. Lett.* **34**, L12706 (2007).
44. Singarayer, J. S. & Valdes, P. J. High-latitude climate sensitivity to ice-sheet forcing over the last 120kyr. *Quat. Sci. Rev.* **29**, 43–55 (2010).
45. Braconnot, P. et al. Results of PMIP2 coupled simulations of the Mid-Holocene and Last Glacial Maximum – Part 1: experiments and large-scale features. *Clim. Past* **3**, 261–277 (2007).
46. Braconnot, P. et al. Evaluation of climate models using palaeoclimatic data. *Nat. Clim. Change* **2**, 417–424 (2012).
47. Campos, M. C. et al. A new mechanism for millennial scale positive precipitation anomalies over tropical South America. *Quat. Sci. Rev.* **225**, 105990 (2019).
48. Erokhina, O. et al. Dependence of slope lapse rate over the Greenland ice sheet on background climate. *J. Glaciol.* **63**, 568–572 (2017).
49. Otto-Bliesner, B. L. & Brady, E. C. The sensitivity of the climate response to the magnitude and location of freshwater forcing: last glacial maximum experiments. *Quat. Sci. Rev.* **29**, 56–73 (2010).
50. He, F. *Simulating Transient Climate Evolution of the Last Deglaciation with CCSM3*. PhD dissertation, Univ. Wisconsin-Madison (2011).
51. Bakker, P., Rogozhina, I., Merkel, U. & Prange, M. Hypersensitivity of glacial summer temperatures in Siberia. *Clim. Past* **16**, 371–386 (2020).
52. Liu, Y. & Chiang, J. C. H. Coordinated abrupt weakening of the Eurasian and North African monsoons in the 1960s and links to extratropical North Atlantic cooling. *J. Clim.* **25**, 3532–3548 (2012).
53. Biasutti, M. et al. Global energetics and local physics as drivers of past, present and future monsoons. *Nat. Geosci.* **11**, 392–400 (2018).
54. Thompson, L. G. et al. Late glacial stage and Holocene tropical ice core records from Huascarán, Peru. *Science* **269**, 46–50 (1995).
55. Thompson, L. G. et al. A 25,000-year tropical climate history from Bolivian ice cores. *Science* **282**, 1858–1864 (1998).
56. Ramirez, E. et al. A new Andean deep ice core from Nevado Illimani (6350 m), Bolivia. *Earth Planet. Sci. Lett.* **212**, 337–350 (2003).
57. Roy, P. D. et al. Late Quaternary paleohydrological conditions in the drylands of northern Mexico: a summer precipitation proxy record of the last 80 cal ka BP. *Quat. Sci. Rev.* **78**, 342–354 (2003).
58. Pausata, F. S. R., Battisti, D. S., Nisancioglu, K. H. & Bitz, C. M. Chinese stalagmite $\delta^{18}O$ controlled by changes in the Indian monsoon during a simulated Heinrich event. *Nat. Geosci.* **4**, 474–480 (2011).
59. Kathayat, G. et al. Indian monsoon variability on millennial-orbital timescales. *Sci. Rep.* **6**, 24374 (2016).
60. Cruz, F. W. Jr et al. Insolation-driven changes in atmospheric circulation over the past 116,000 years in subtropical Brazil. *Nature* **434**, 63–66 (2005).
61. Carlson, A. E. et al. Subtropical Atlantic salinity variability and Atlantic meridional circulation during the last deglaciation. *Geology* **36**, 991–994 (2008).
62. DiNezio, P. N. et al. Synthesis of hydroclimate changes during Heinrich Stadial 1. *Zenodo* https://doi.org/10.5281/zenodo.13881535 (2024).
63. Vecchi, G. A. & Soden, B. J. Global warming and the weakening of the tropical circulation. *J. Clim.* **20**, 4316–4340 (2007).
64. Merkel, U., Prange, M. & Schulz, M. ENSO variability and teleconnections during glacial climates. *Quat. Sci. Rev.* **29**, 86–100 (2010).
65. Kageyama, M. et al. Mid-holocene and Last Glacial Maximum climate simulations with the IPSL model—part I: Comparing IPSL_CM5A to IPSL_CM4. *Clim. Dyn.* **40**, 2447–2468 (2013).
66. Zhang, X., Lohmann, G., Knorr, G. & Xu, X. Different ocean states and transient characteristics in last glacial maximum simulations and implications for deglaciation. *Clim. Past* **9**, 2319–2333 (2013).
67. Chikamoto, M. O., Abe-Ouchi, A., Oka, A., Ohgaito, R. & Timmermann, A. Quantifying the ocean's role in glacial CO_2 reductions. *Clim. Past* **8**, 545–563 (2012).
68. Osman, M. B. et al. Globally resolved surface temperatures since the Last Glacial Maximum. *Nature* **599**, 239–244 (2021).
69. Zhao, M., Beveridge, N. A. S., Shackleton, N. J., Sarnthein, M. & Eglinton, G. Molecular stratigraphy of cores off northwest Africa: sea surface temperature history over the last 80 Ka. *Paleoceanography* **10**, 661–675 (1995).
70. Schmidt, M. W., Spero, H. J. & Lea, D. W. Links between salinity variation in the Caribbean and North Atlantic thermohaline circulation. *Nature* **428**, 160–163 (2004).
71. Crivellari, S. et al. Thermal response of the western tropical Atlantic to slowdown of the Atlantic meridional overturning circulation. *Earth Planet. Sci. Lett.* **519**, 120–129 (2019).

72. Rühlemann, C., Mulitza, S., Müller, P. J., Wefer, G. & Zahn, R. Warming of the tropical Atlantic Ocean and slowdown of thermohaline circulation during the last deglaciation. *Nature* **402**, 511–514 (1999).
73. Herbert, T. D. & Schuffert, J. D. Alkenone unsaturation estimates of sea-surface temperatures at site 1002 over a full glacial cycle. *Proc. ODP Sci. Results* **165**, 239–247 (2000).
74. Lea, D. W., Pak, D. K., Peterson, L. C. & Hughen, K. A. Synchroneity of tropical and high-latitude Atlantic temperatures over the last glacial termination. *Science* **301**, 1361–1364 (2003).
75. Reißig, S., Nürnberg, D., Bahr, A., Poggemann, D.-W. & Hoffmann, J. Southward displacement of the North Atlantic subtropical gyre circulation system during North Atlantic cold spells. *Paleoceanogr. Paleoclimatol.* **34**, 866–885 (2019).
76. Schmidt, M. W. et al. Impact of abrupt deglacial climate change on tropical Atlantic subsurface temperatures. *Proc. Natl Acad. Sci. USA* **109**, 14348–14352 (2012).
77. Kim, J.-H. et al. Pronounced subsurface cooling of North Atlantic waters off northwest Africa during Dansgaard–Oeschger interstadials. *Earth Planet. Sci. Lett.* **339–340**, 95–102 (2012).
78. Bahr, A. et al. Low-latitude expressions of high-latitude forcing during Heinrich Stadial 1 and the Younger Dryas in northern South America. *Glob. Planet. Change* **160**, 1–10 (2018).
79. DiNezio, P. N. Matlab code to reproduce results from "Tropical response to ocean circulation slowdown raises future drought risk" by DiNezio et al. (2025). *Zenodo* https://doi.org/10.5281/zenodo.13886977 (2025).

Acknowledgements We acknowledge the decades of work by many individual authors who produced the palaeoclimate records used here. We thank K. Thirumalai for comments on this work. We acknowledge A. Abe-Ouchi, G. Lohmann and J. Singarayer for providing model output and N. Piatrunia and K. Gomez for participating in an initial collation of palaeoclimate records. The CESM project is supported primarily by the National Science Foundation (NSF). This work was supported by the NCAR, which is a main facility sponsored by the NSF under cooperative agreement no. 1852977. Computing and data storage resources, including the Cheyenne supercomputer (https://doi.org/10.5065/D6RX99HX), were provided by the Computational and Information Systems Laboratory at NCAR. We thank all the scientists, software engineers and administrators who contributed to the development of CESM1. Funding for this work was provided by the NSF (grants AGS-2002528 and AGS–2103007 for P.N.D., grants AGS-2002528 and OCE–1903482 for T.S.). M.K. was funded by the CNRS (Centre National de la Recherche Scientifique). The IPSL model was run on the Très Grande Infrastructure de Calcul at Commissariat à l'Energie Atomique (gen2212 project). M.P. and U.M. acknowledge the support from the PalMod project (www.palmod.de; FKZ 01LP1915B and 01LP1916C) funded by the German Federal Ministry of Education and Research. X.Z. acknowledges the technical support of the National Large Scientific and Technological Infrastructure Earth System Numerical Simulation Facility (https://cstr.cn/31134.02.EL), and the support from National Key Research and Development Projects of China (2023YFF0805201).

Author contributions P.N.D. and T.M.S. conceived the study and wrote the paper. T.M.S., P.N.D., A.L. and C.S. compiled and analysed the palaeodata. P.N.D., T.M.S. and D.L. formulated the hypotheses. P.N.D., T.S. and X.W. analysed the model output. P.N.D., M.K., U.M., M.P., B.O.-B. and X.Z. performed the simulations.

Competing interests The authors declare no competing interests.

Additional information

Supplementary information The online version contains supplementary material available at https://doi.org/10.1038/s41586-025-09319-x.

Correspondence and requests for materials should be addressed to Pedro N. DiNezio.

Peer review information *Nature* thanks Yassine Ait Brahim, Matthew Osman and Frerk Pöppelmeier for their contribution to the peer review of this work. Peer reviewer reports are available.

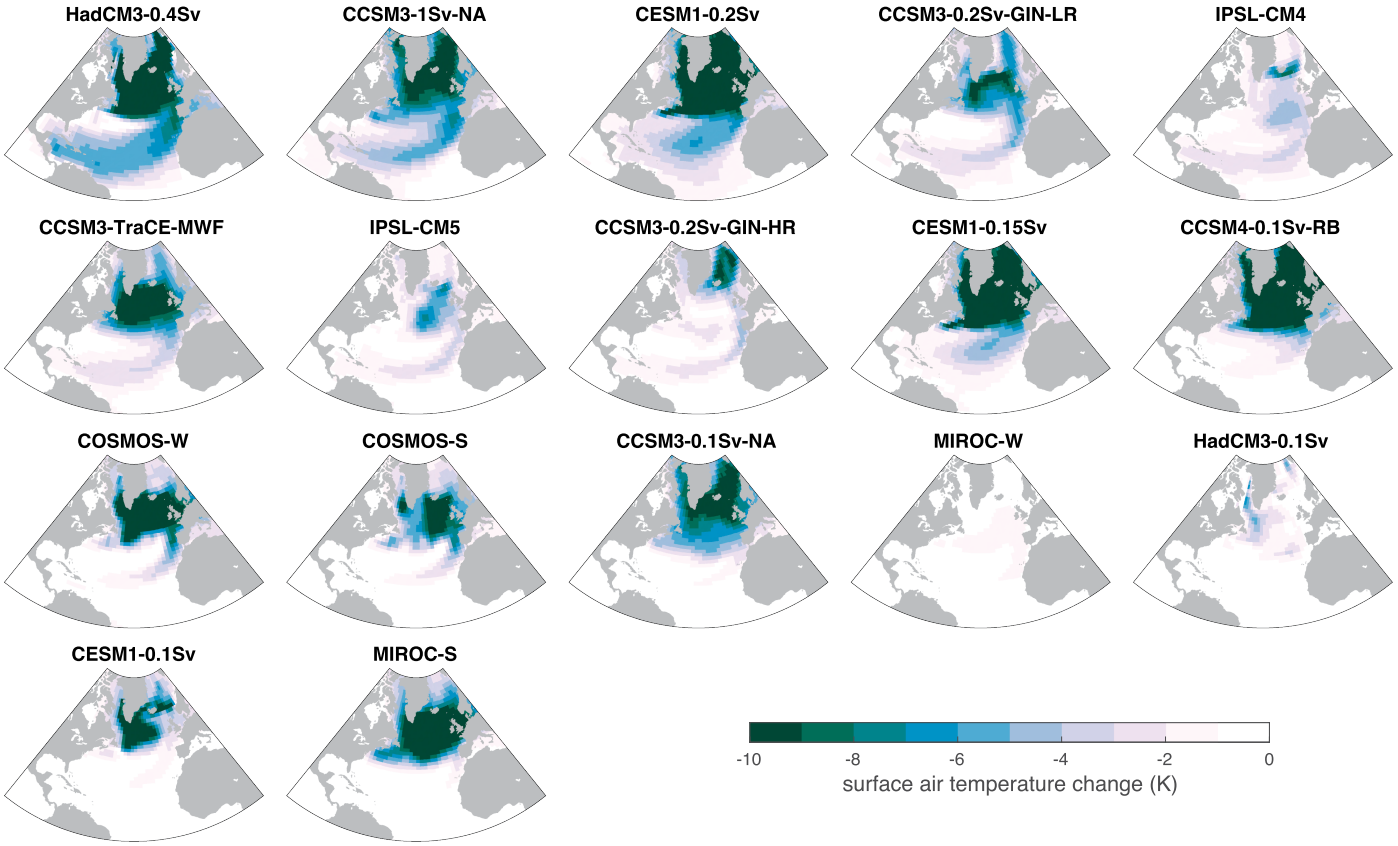

Extended Data Fig. 1 | Simulated changes in surface air temperature in response to freshwater forcing. Change in annual-mean surface air temperature simulated by climate models under varied magnitudes and locations of freshwater forcing in the North Atlantic. The maps are labeled according to the name of the simulation as specified in Extended Data Table 1. All experiments were run relative to glacial background states. The climate response to freshwater forcing was computed as difference relative to the corresponding glacial simulation as described in the Methods.

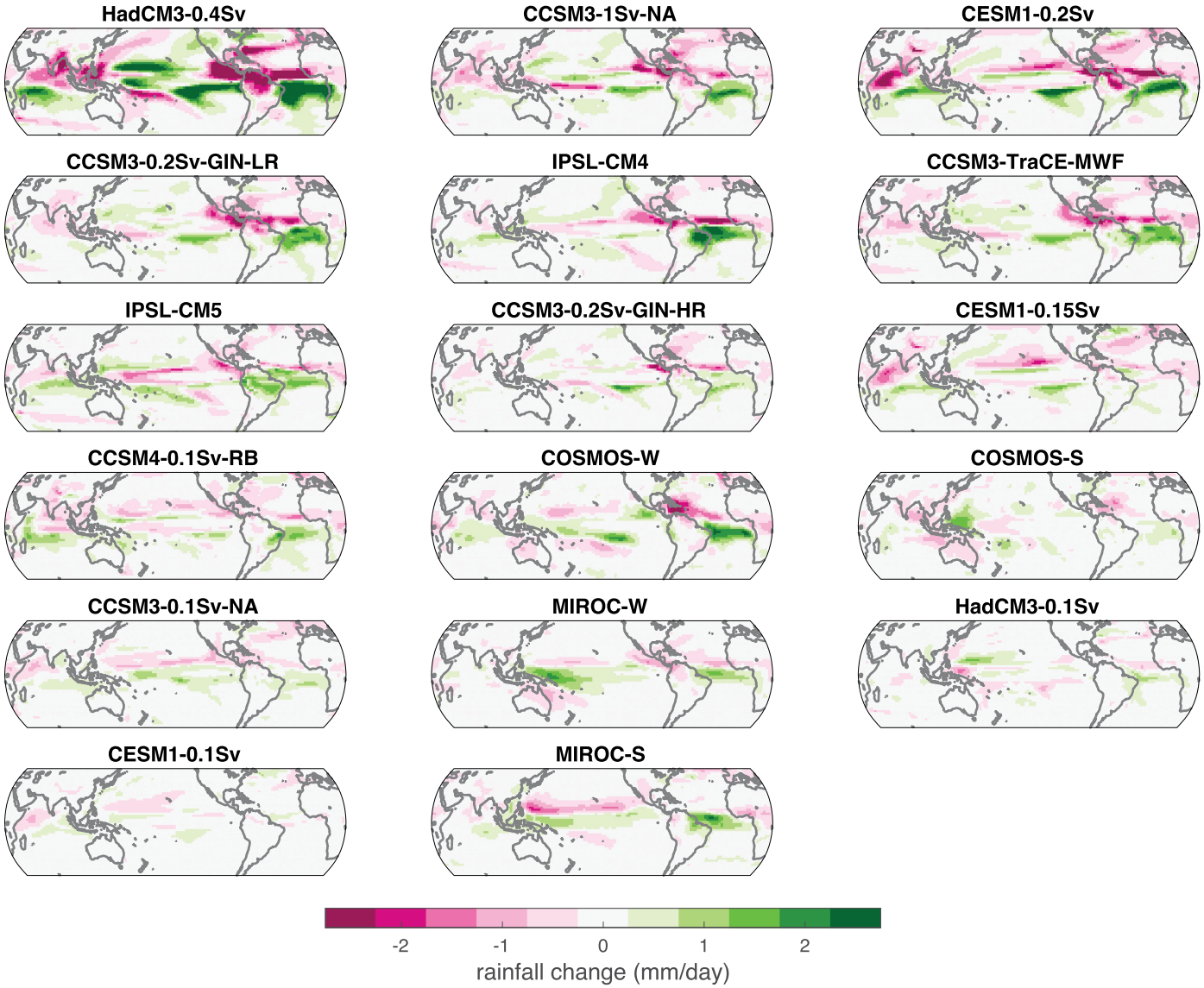

Extended Data Fig. 2 | Simulated changes in rainfall in response to freshwater forcing. Change in annual-mean rainfall simulated by climate models under varied magnitudes and locations of freshwater forcing in the North Atlantic. The maps are labeled according to the name of the simulation as specified in Extended Data Table 1. All experiments were run relative to glacial background states. The climate response to freshwater forcing was computed as difference relative to the corresponding glacial simulation as described in the Methods.

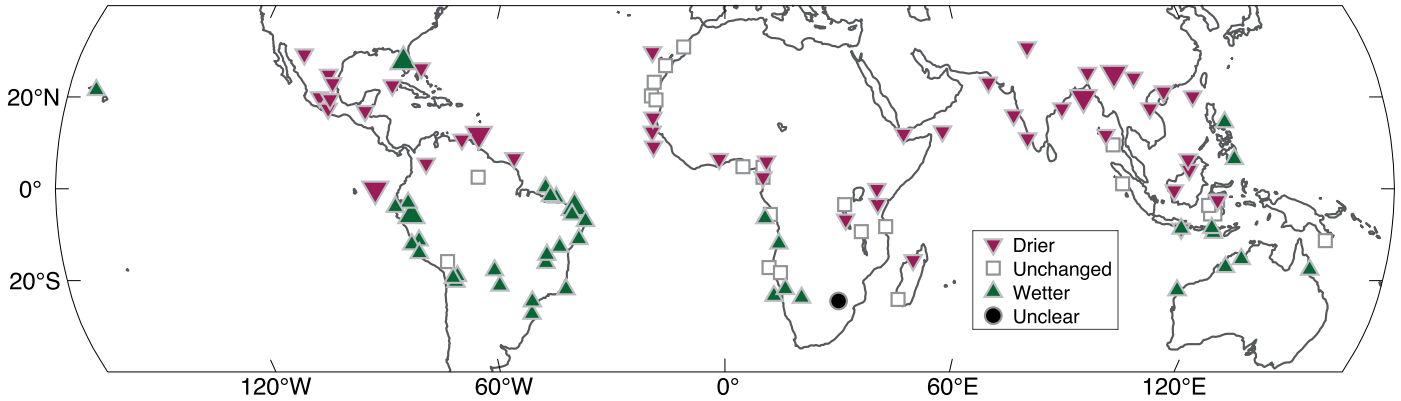

Extended Data Fig. 3 | Reconstructed hydroclimate changes during Heinrich Stadial 1. Proxy-inferred hydroclimate changes during Heinrich Stadial 1 (symbols) from published palaeoclimate records capturing drier (red downward triangle), unchanged (white squares), wetter (green upward triangle), or unclear (black circles) conditions during Heinrich Stadial 1. Bigger triangles indicate sites resulting from merging multiple records within a 100 km radius.

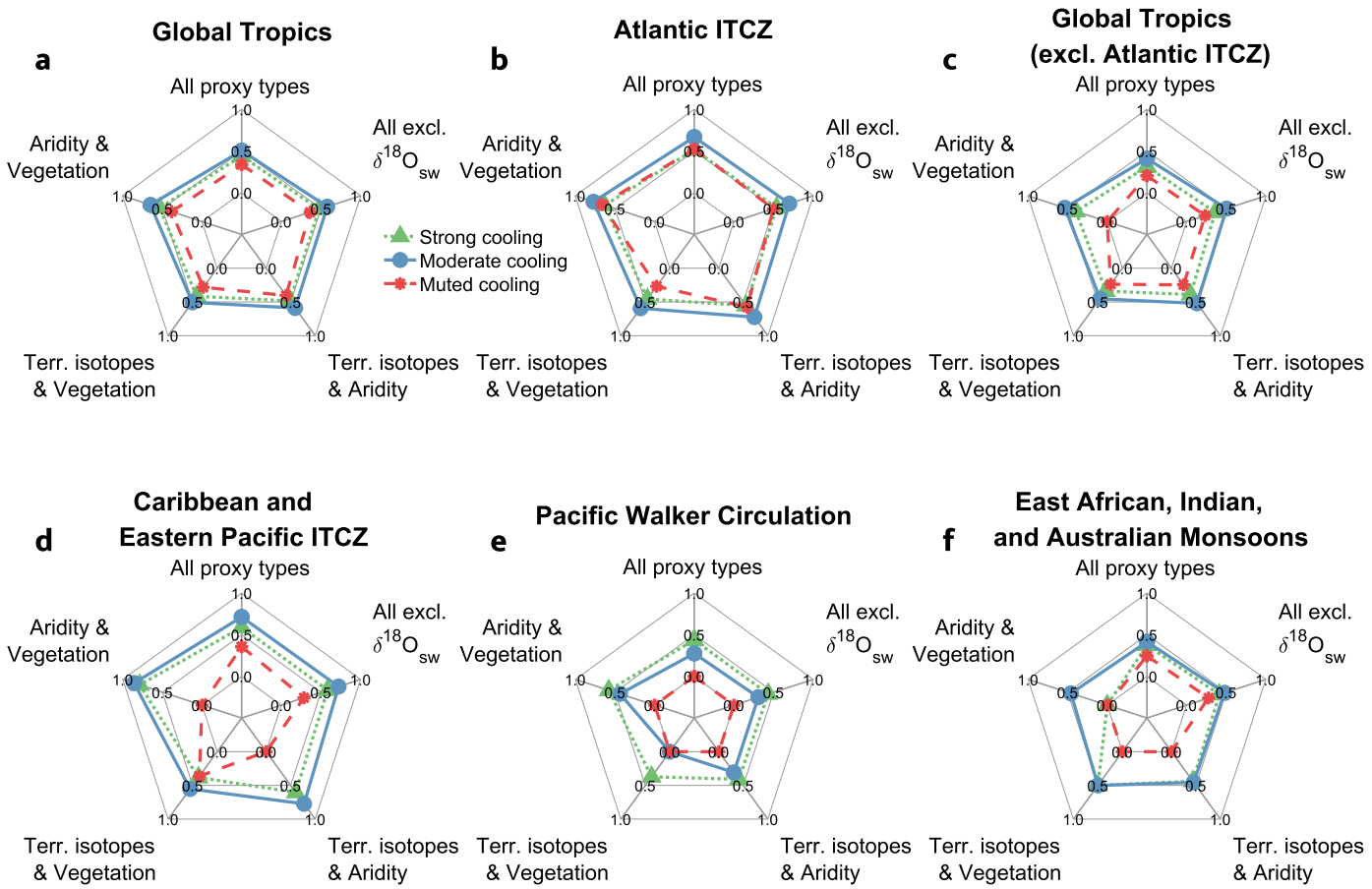

Extended Data Fig. 4 | Sensitivity of global and regional proxy-model agreement to different proxy types. Global (**a**) and regional (**b**–**f**) agreement between hydroclimate changes reconstructed using different combinations of two proxy types and the simulated responses associated with cooling patterns in the North Atlantic. Dotted, solid, and dashed lines correspond to ensemble-mean responses from simulations with stronger, moderate, and muted cooling over the tropical North Atlantic respectively. Model-proxy agreement is quantified using the Cohen's κ metric.

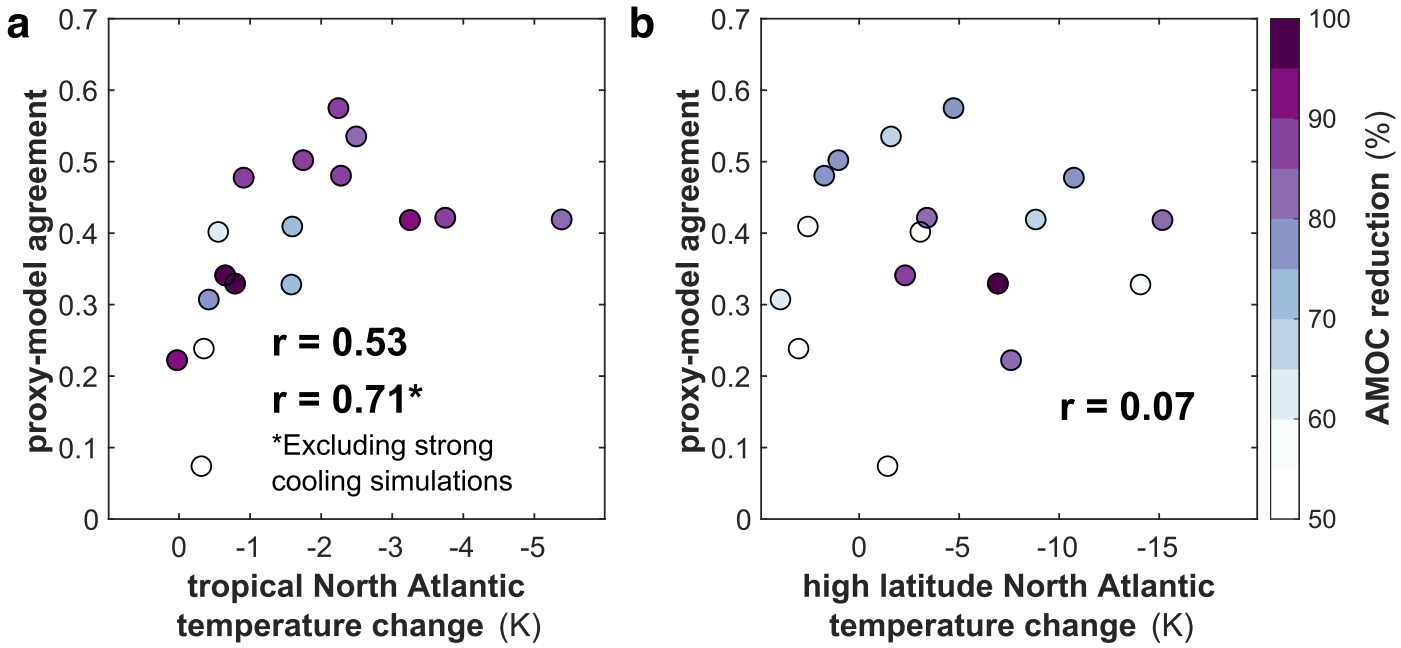

Extended Data Fig. 5 | Correlation between simulated responses associated with AMOC reductions and global proxy-model agreement for hydroclimate changes. a. Correlation between proxy-model agreement and simulated tropical North Atlantic temperature change. **b**. Correlation between proxy-model agreement and simulated high latitude North Atlantic temperature change. Each symbol represents a simulation in our ensemble. Symbol colors indicate the magnitude of the AMOC reduction as % of the strength in the glacial baseline.

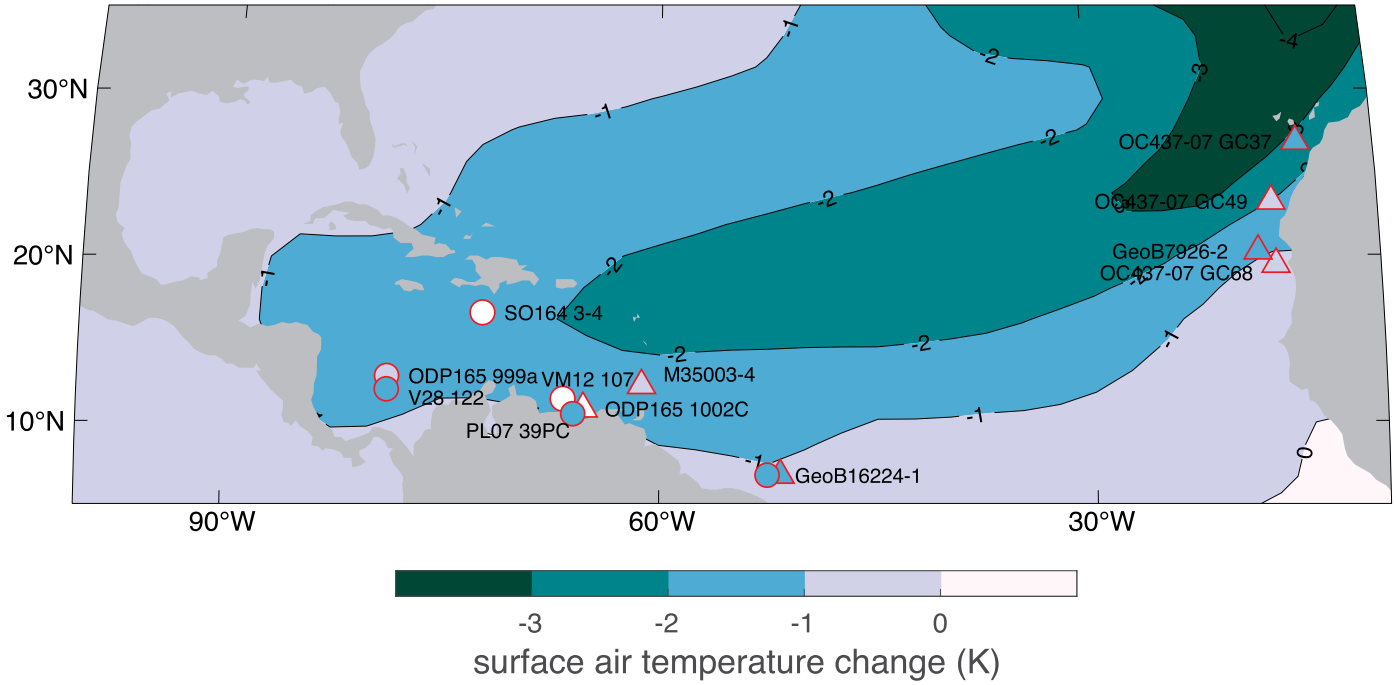

Extended Data Fig. 6 | Simulated and reconstructed patterns of cooling over the tropical North Atlantic. Changes in surface air temperature from simulations classified as moderate tropical North Atlantic cooling (shading) and inferred for HS1 using existing temperature records (symbols). Triangles correspond to $U^{k'}_{37}$ records and circles to Mg/Ca records. White symbols indicate a muted temperature response during HS1. Symbols are colored based on the categories listed in Extended Data Table 2 following the same color scheme as for the simulated changes.

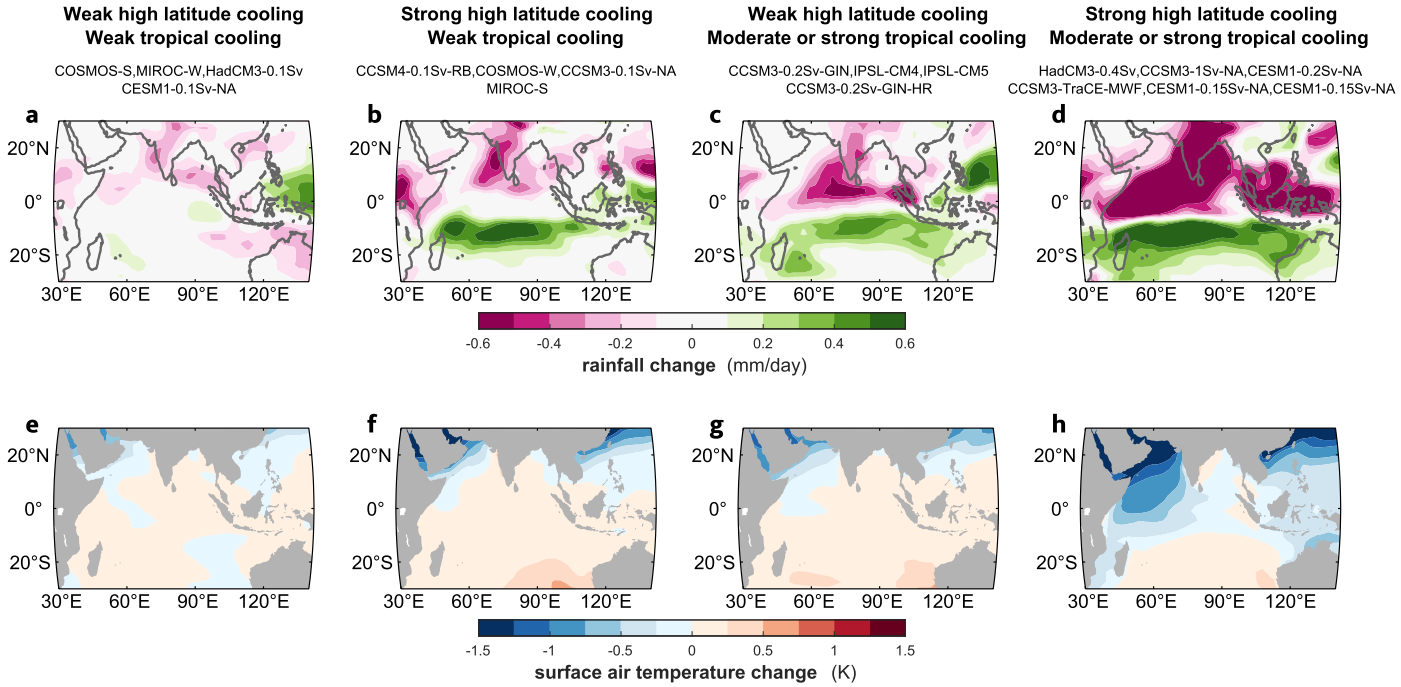

Extended Data Fig. 7 | Climate responses in the Indian Ocean for different patterns of cooling in the North Atlantic. Changes in annual-mean rainfall **(a–d)** and surface air temperature **(e–h)** averaged across simulations with different combinations of strong and muted cooling in the high latitude and tropical North Atlantic. The simulations in each group are listed below each panels title. The values of strong and weak high latitude cooling range from −20 to −8 K and from −7 to −1 K respectively. The values of strong/moderate and weak tropical cooling range from −5.5 to −1 K and from −1 to 0 K respectively.

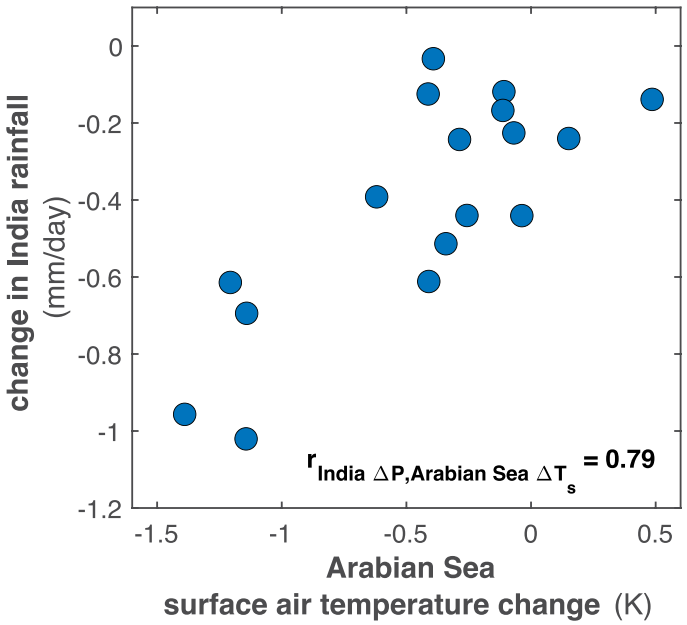

Extended Data Fig. 8 | Correlation between changes in rainfall over India and Arabian Sea cooling. Relationship between rainfall changes over India (70–85°E 7–30°N) (y-axix) vs. the magnitude of the surface air temperature responses over the Arabian Sea (50–70°E 5–25°N).

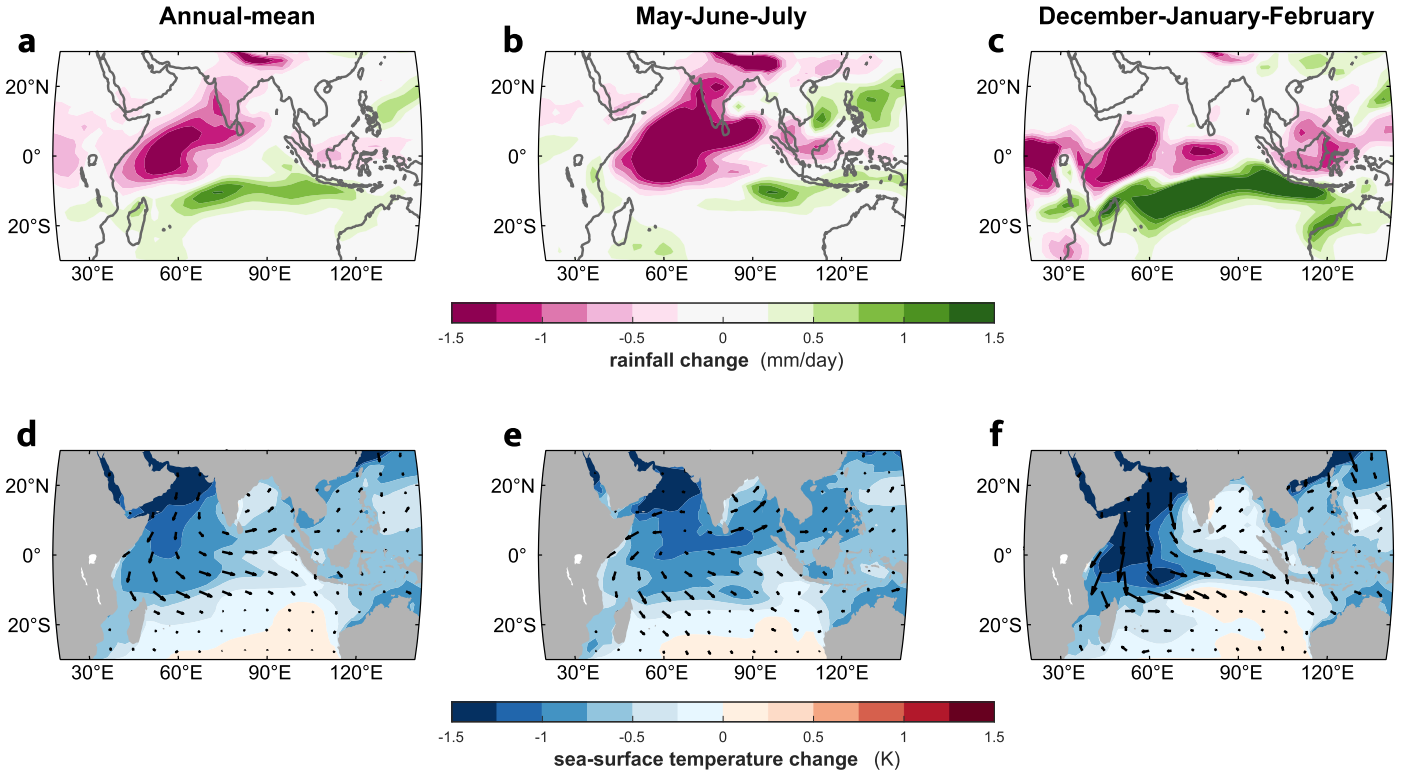

Extended Data Fig. 9 | Seasonal climate responses in the Indian Ocean. Changes in rainfall (**a**–**c**) and surface air temperature (**d**–**f**) simulated by the Community Earth System Model Version 1 (CESM1) in response to 0.15 Sv of freshwater forcing. Annual mean (**a**,**d**), boreal summer (**b**,**e**) and austral summer (**c**,**f**) changes are displayed to illustrate the responses of the Indian and Australian summer monsoons respectively. Vectors indicate changes in surface wind stress.

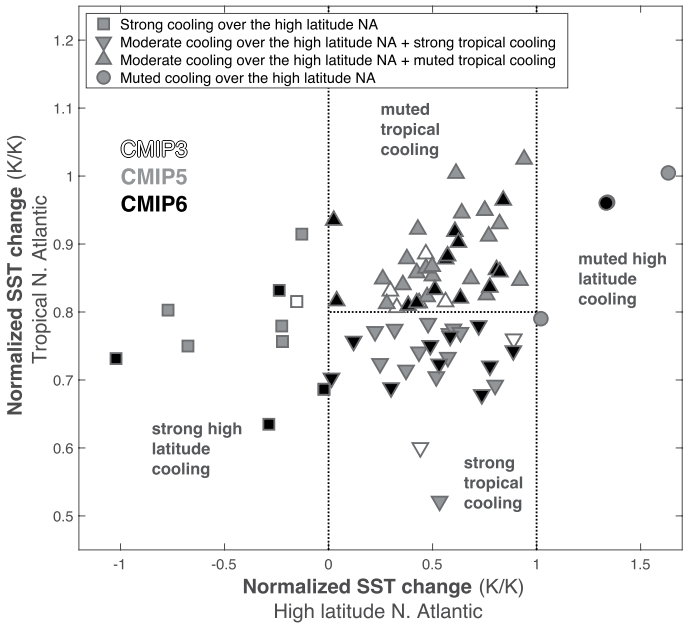

Extended Data Fig. 10 | AMOC-related sea-surface temperature changes in CMIP greenhouse warming simulations. Normalized sea-surface temperature change over the high latitude (x-axis) vs. tropical (y-axis) North Atlantic simulated from 1921 to 2100 under high-emissions scenarios by models participating in the Climate Model Intercomparison Project (CMIP). Each symbol corresponds to values simulated by a distinct model participating in phases 3, 5, and 6 of CMIP indicated by the colors. Models are grouped based on the magnitude of the normalized sea-surface temperature change in each region defined by the dotted lines and by the symbols as indicated by the legend. The averaged sea-surface temperature change over the North Atlantic (50°W–0°50°N–65°N) is normalized by the surface temperature change averaged over the Northern Hemisphere (0–90°N). The averaged sea-surface temperature change over the tropical North Atlantic (80°W–40°W 12°N–22°N) is normalized by the surface temperature averaged change over the tropics (20°S-20°N).

Extended Data Table 1 | Freshwater hosing simulations and model configuration

Simulation	Reference	Ice sheet reconstruction	Model resolution		FW forcing		AMOC reduction (Sv)	TNA cooling (K)
			Atmosphere	Ocean	Rate (Sv)	Loc.		
Simulations with strong cooling over the tropical N. Atlantic								
HadCM3-0.4Sv	44	ICE-5G (24 ka)	3.75 × 2.5°L19	1.25°	0.4	NA	15.1	-5.4
CCSM3-1Sv-NA	49	ICE-5G	2.8 × 2.8°L26	1°	1	NA	12.0	-3.8
CESM1-0.2Sv	this work	PMIP3	2.5 × 1.9°L30	1°L54	0.2	NA	14.9	-3.2
Simulations with moderate cooling over the tropical N. Atlantic								
CCSM3-0.2Sv-GIN-LR	64	ICE-5G	3.75 × 3.75°L26	3°L25	0.2	GIN	6.6	-2.4
IPSL-CM4	40	ICE-5G	3.75 × 2.5°L19	2°L31	0.1	NA	10.0	-2.2
CCSM3-TraCE-MWF	41	ICE-5G	3.75 × 3.75°L26	3°L25	0.17	NA	9.5	-2.2
IPSL-CM5	65	PMIP3	3.75 × 1.8°L39	2°L31	0.1	NA	12.5	-1.7
CCSM3-0.2Sv-GIN-HR	47, 48	ICE-5G	1.4 × 1.4°L26	1°L40	0.2	GIN	6	-1.6
CESM1-0.15Sv	this work	PMIP3	2.5 × 1.9°L30	1°L54	0.15	NA	10.5	-1.6
Simulations with muted cooling over the tropical N. Atlantic								
CCSM4-0.1Sv-RB	51	GLAC-D	2.5 × 1.9°L26	1°L60	0.1	RB	18	-0.9
COSMOS-W	66	PMIP3	3.75 × 3.75°L19	3 × 1.8°	0.2	RB	17.9	-0.8
COSMOS-S	66	PMIP3	3.75 × 3.75°L19	3 × 1.8°	0.2	RB	23.9	-0.6
CCSM3-0.1Sv-NA	49	ICE-5G	2.8 × 2.8°L26	1°	0.1	NA	6.2	-0.6
MIROC-W	67	ICE-5G	2.8 × 2.8°L20	1.4°	0.1	NA	5.4	-0.4
HadCM3-0.1Sv	44	ICE-5G (24 ka)	3.75 × 2.5°L19	1.25°	0.1	NA	4.5	-0.3
CESM1-0.1Sv	this work	PMIP3	2.5 × 1.9°L30	1°L54	0.1	NA	4.7	-0.3
MIROC-S	67	ICE-5G	2.8 × 2.8°L20	1.4°	0.1	NA	16.0	0.1

The simulations are named so that they can be distinguished based on the model used, the rate and location of freshwater forcing, and the state of the AMOC in the control simulation[64–67]. W = weak AMOC in the control simulation and S = strong AMOC in the control simulation. NA = North Atlantic (50–70°N), GIN = Greenland-Iceland-Norwegian Seas (north of about 65°N), RB = Ruddiman Belt (i.e., North Atlantic, 40-50°N).

Extended Data Table 2 | Temperature records used to infer the pattern and magnitude of tropical Atlantic cooling during Heinrich Stadial 1

Core	Proxy	Latitude (°N)	Longitude (°W)	HS1 response	Reference
OC437-07 GC49	$U_{37}^{k'}$	17.4	23.2	< 1	68
OC437-07 GC68	$U_{37}^{k'}$	17.3	19.4	< 1	68
OC437-07 GC37	$U_{37}^{k'}$	15.4	26.8	> 1	68
ODP165 999a	Mg/Ca	78.7	12.7	< 1	70
GeoB16224-1	$U_{37}^{k'}$	52.1	6.7 2	> 1	71
GeoB16224-1	Mg/Ca	52.1	6.7 2	> 1	71
M78-1 235-1	Mg/Ca	61.0	11.6	N/A	78
M35003-4	$U_{37}^{k'}$	61.2	12.1	< 1	72
ODP108 658C	$U_{37}^{k'}$	18.6	20.7	N/A	69
ODP165 1002C	$U_{37}^{k'}$	65.2	10.7	0	73
PL07 39PC	Mg/Ca	65.9	10.7	> 1	74
SO164 3-4	Mg/Ca	72.2	16.5	0	75
VM12 107	Mg/Ca	66.6	11.3	0	76
VM28 122	Mg/Ca	78.7	11.9	> 1	70
GeoB7926-2	$U_{37}^{k'}$	18.5	20.2	> 1	77

Inference of range of cooling at each site during Heinrich Stadial 1 relative to the deglacial background[68–78]. The values indicate: 0 = No evidence of cooling, <1 = Evidence of cooling less than 1 K, >1 = Evidence of cooling larger than 1 K (but not larger than 2 K), N/A = excluded record due to issues outlined in Section 3 of the Supplementary Methods.